Heliyon 10 (2024) e31703

Contents lists available at ScienceDirect

Heliyon

journal homepage: www.cell.com/heliyon

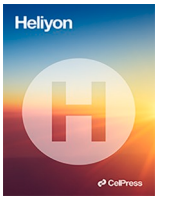

Review article

# Surface engineering of pure magnesium in medical implant applications

Mengqi Gong [a,b], Xiangjie Yang [a,b,*], Zhengnan Li [c], Anshan Yu [a,b,d,e], Yong Liu [a,f], Hongmin Guo [b,c], Weirong Li [d], Shengliang Xu [a,b], Libing Xiao [a,b], Tongyu Li [a,b], Weifeng Zou [a,b]

[a] School of Advanced Manufacturing, Nanchang University, Nanchang, 330031, China
[b] Key Laboratory of Near Net Forming in Jiangxi Province, Nanchang, 330031, China
[c] School of Physics and Materials Science, Nanchang University, Nanchang, 330031, China
[d] Dongguan Magna Medical Devices Co., Ltd., Dongguan, 523808, China
[e] School of Mechanical and Electrical Engineering, Jinggangshan University, Ji'an, 343009, China
[f] Key Laboratory of Lightweight and High Strength Structural Materials of Jiangxi Province, Nanchang, 330031, China

ARTICLE INFO

*Keywords:*
Pure magnesium
Surface modification methods
Corrosion resistance
Biocompatibility

ABSTRACT

This review comprehensively surveys the latest advancements in surface modification of pure magnesium (Mg) in recent years, with a focus on various cost-effective procedures, comparative analyses, and assessments of outcomes, addressing the merits and drawbacks of pure Mg and its alloys. Diverse economically feasible methods for surface modification, such as hydrothermal processes and ultrasonic micro-arc oxidation (UMAO), are discussed, emphasizing their exceptional performance in enhancing surface properties. The attention is directed towards the biocompatibility and corrosion resistance of pure Mg, underscoring the remarkable efficacy of techniques such as Ca-deficientca-deficient hydroxyapatite (CDHA)/$MgF_2$ bi-layer coating and UMAO coating in electrochemical processes. These methods open up novel avenues for the application of pure Mg in medical implants. Emphasis is placed on the significance of adhering to the principles of reinforcing the foundation and addressing the source. The advocacy is for a judicious approach to corrosion protection on high-purity Mg surfaces, aiming to optimize the overall mechanical performance. Lastly, a call is made for future in-depth investigations into areas such as composite coatings and the biodegradation mechanisms of pure Mg surfaces, aiming to propel the field towards more sustainable and innovative developments.

## 1. Introduction

### 1.1. Metallic implants

The progression of metallic implants is significantly influenced by the need for advanced bone repair techniques, especially in addressing long bone fractures. Metals are pivotal in various orthopedic devices, serving in both temporary solutions like bone plates, nails, and screws, as well as permanent implants such as total joint replacements. Moreover, metals play a crucial role in dental and

* Corresponding author. School of Advanced Manufacturing, Nanchang University, Nanchang, 330031, China.
*E-mail address:* yangxj@ncu.edu.cn (X. Yang).

https://doi.org/10.1016/j.heliyon.2024.e31703
Received 4 March 2024; Received in revised form 18 April 2024; Accepted 21 May 2024
Available online 23 May 2024

orthodontic applications, spanning from dental fillings to root canals [1–3]. Recent investigations into metal biomaterials have progressively shifted their focus towards innovative reconstructive procedures for hard tissues and organs. Examples include the application of nickel-titanium (NiTi) shape memory alloy in vascular stents and [4–8], and the exploration of novel magnesium (Mg)-based alloys for advancements in bone tissue engineering and regeneration [9–14]. The design and selection of metallic implants depend on their specific medical applications. In order to ensure safety and freedom from rejection reactions over an appropriate period, ideal metallic implants should exhibit essential traits, including, but not confined to: (1) exceptional biocompatibility (non-toxicity), (2) requisite corrosion resistance, (3) appropriate mechanical properties, (4) elevated wear resistance, and (5) mechanisms conducive to osseointegration.

Among the various commonly used medical metal implants, Mg and its alloys demonstrate outstanding mechanical characteristics, biodegradability, and the ability for degradation by-products to be metabolically excreted from the body without adverse effects [15–18]. Currently, medical Mg implants primarily include Mg alloys such as WE43 [19–24], AZ31 [25–29], Mg-Ca [30–33], and MgZnCa [34–36]. However, the incorporation of other metallic elements into Mg alloys does not necessarily ensure favorable biocompatibility of these added elements and complete in vivo degradation. In utilizing pure Mg as an implant material, researchers are predominantly exploring surface synthesis coatings [37–39], micro-arc oxidation (MAO) [40,41], and hydrothermal treatment [42–44]. The research findings indicate that surface modification of pure Mg materials effectively reduces their degradation rate, but still cannot match the clinical fracture healing time. Additionally, pure Mg is prone to pitting corrosion, faster degradation rates, uncontrollable degradation behavior, and the occurrence of postoperative inflammation due to hydrogen evolution during degradation, especially in human environments with high chloride ion content. These unresolved issues significantly limit the clinical application of commercial pure Mg. In theory, an optimal degradable Mg material should retain stability during the initial stages of implantation and undergo rapid degradation following the complete healing of the repair area. This approach helps eliminate the necessity for a secondary surgical intervention.

### *1.2. A distinctive metal*

Mg, boasting a density of 1.74 g/cm$^3$, stands out as the lightest among engineering metals. This value is notably lower compared to aluminum (Al, 2.70 g/cm$^3$), Ti (4.51 g/cm$^3$), and iron (Fe, 7.87 g/cm$^3$) [45]. While Mg boasts the highest strength-to-weight ratio among structural alloys, ongoing research delves into the comprehensive understanding of its properties, including corrosion resistance, ductility, and creep behavior. Noteworthy attributes of Mg encompass exceptional damping capacity, environmental and human body non-toxicity (making it an excellent choice for biodegradable implants), ease of high-speed milling and turning operations (e.g., tool life 5–10 times longer than Al), and versatility through processes like rolling and extrusion. Despite these advantages and considering the moderate cost (especially per unit volume), the adoption of Mg and its alloys remains somewhat constrained [46–48].

In recent years, there has been an increasing acceptance of implants made from Mg for treating patients. This type of metallic biomaterial possesses the capability to achieve in-situ functionality while exhibiting the inherent ability to self-degrade within the body [49]. The unique properties of Mg and its alloys as implant materials have garnered widespread attention and research. Mg is an essential trace element for the human body, characterized by its excellent absorbability and biocompatibility. With a density and elastic modulus closely resembling those of bones, Mg effectively avoids stress shielding effects. In the field of orthopedics, Mg metal implants find application in fracture repair and bone defect treatment, gradually degrading over time to stimulate bone tissue regeneration [50,51]. In the cardiovascular domain, Mg metal implants serve as materials for vascular stents. Their biodegradability allows the implant to adapt to physiological changes in blood vessels, alleviating vascular stress and mitigating potential complications associated with long-term stent use [52]. In dental restoration, Mg metal implants also demonstrate potential applications [53,54]. The combination of biodegradability and excellent mechanical properties positions Mg as a promising material for dental implant therapy. As an innovative biomaterial, Mg metal implants showcase tremendous prospects in the medical field, offering sustainable and personalized solutions for clinical treatments through continuous research and innovation.

Future research directions may include, but are not limited to, the following aspects.

1. Material modification: utilize surface treatments and coating technologies to further optimize the performance of Mg metal implants. Enhance their biocompatibility and mechanical properties through rational material modifications.
2. Expansion of clinical applications: explore the potential of Mg metal implants in other clinical domains, such as neurosurgery and plastic surgery, to provide effective treatment solutions for a broader patient population.
3. Biodegradation mechanism studies: conduct in-depth investigations into the biodegradation mechanisms of Mg metal implants in vivo. This will provide a scientific basis for more precise control over degradation rates and release processes.
4. Interdisciplinary collaboration: foster collaboration across disciplines, including medicine, biomaterials, and engineering, to collectively advance research and applications of Mg metal implants. This collaborative effort aims to offer patients safer and more effective treatment options.

### *1.3. Historical of surface treatment of pure Mg implants*

Mg metal was first isolated by Sir Humphry Davy in 1808 and achieved commercial production in 1852 [55]. In 1878, Huse was the first to observe the biodegradable characteristics of Mg and conducted studies on its corrosion behavior. He used Mg wire as ligatures for hemostasis in human patients [56]. However, many surgeons noted the rapid corrosion of Mg and the associated hydrogen release, raising questions about its biocompatibility. In 1969, David A. Vermilyea deposited a layer of $Mg(OH)_2$ film on the surface of pure Mg

without using inhibitors. He detected a tenfold reduction in the overall metal removal rate at pH 9–10 [57]. Since the latter half of the 20th century until the present, there has been a sustained and growing interest in the corrosion resistance of pure Mg surfaces [41, 58–89]. Key advancements in pure Mg corrosion are illustrated in Fig. 1. It is noteworthy that the significant surge in activity over the past two decades indicates the existence of some major unresolved issues. Amy L. Rudd and colleagues, in the year 2000, subjected pure Mg to a treatment in a solution containing cerium, lanthanum, and praseodymium [90]. This treatment significantly enhanced the corrosion resistance of Mg in a solution with a pH of 8.5. However, the coating began to deteriorate with prolonged immersion in the corrosive test solution, indicating a relatively short-term effectiveness in corrosion resistance. Additionally, the decomposition and absorption of rare earth elements in the body may pose unknown allergic reactions. The surfaces of biomaterials such as ceramics, metals, and polymers can be nano-functionalized through various surface modification techniques. Nano-functionalized surfaces can significantly impact cellular and subcellular functions, exhibiting favorable biological characteristics. However, to achieve more precise control over surface nanostructures, it is essential to develop improved and simpler technologies. Additionally, evaluating the safety of nano-functional surfaces before clinical applications is crucial [91–93].

In the realm of future surface modification for pure Mg and Mg alloys, the exploration of composite coatings is regarded as a pivotal research avenue compared to single coatings [94–97]. In 2018, Feng Peng and collaborators achieved the creation of a super-hydrophobic, highly adhesive coating on pure Mg surfaces using a straightforward one-step method, drawing inspiration from the "petal effect" [80]. The coating displays outstanding corrosion resistance and efficiently prevents platelet adhesion, reducing hemolysis to levels suitable for clinical applications. It holds promising clinical prospects. In 2023, Jieyang Dong et al. employed an immersion method and MAO to fabricate a poly(1,3-trimethylene carbonate) (PTMC) and polydopamine (PDA) bilayer, and MAO composite coating on Mg surfaces [98]. This composite coating exhibits excellent corrosion resistance and biocompatibility. The research shows potential for charting a new course in the design of innovative degradable Mg-based implants for orthopedic applications. This paper reviews the latest advancements and current scientific challenges in pure Mg coatings in recent years, focusing on methods, structures, and performance.

## 2. Surface modified pure Mg bioimplants

Currently, primary Mg alloys employed in medical implants include WE43, AZ31, Mg–Ca and MgZnCa. Since Mg alloys are doped with other metal elements, there is no guarantee that the added elements are biocompatible and completely degraded in vivo. To

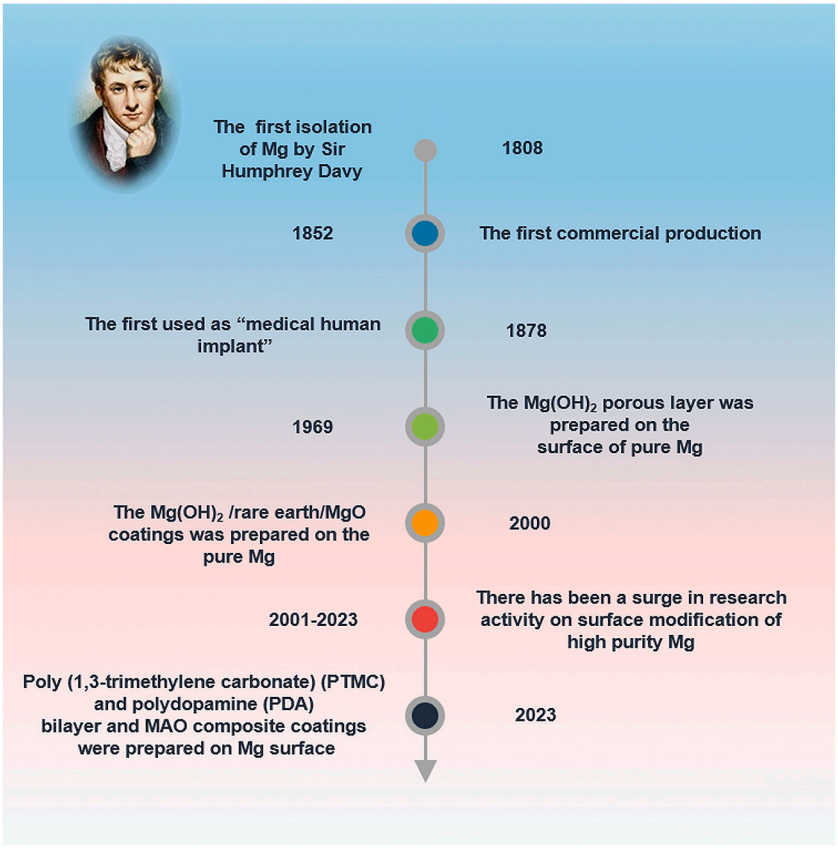


**Fig. 1.** The technological development timeline of corrosion studies on pure Mg and surface-modified pure Mg.

utilize pure Mg as an implant material, its surface will be chemical treatment, electrochemical treatment, mechanical treatment etc. to synthesize the coating. Surface-modified pure Mg materials play a dual role by efficiently minimizing the body's absorption of extraneous elements and concurrently contributing to a decelerated degradation rate of implants within the body.

### 2.1. Chemical methods

Mainstream chemical methods for surface modification of pure Mg include chemical conversion coating technology, hydrothermal treatment, alkali-heat treatment, anodic oxidation, plasma electaolyte oxidation (PEO/MAO), and some advanced coating technologies. The hydrothermal and alkali-heat treatment can also be classified as chemical conversion coating technology, both anodic oxidation and PEO are electrochemical treatment.

#### 2.1.1. Chemical conversion coating technology

Chemical conversion coatings are produced through the interplay of chemical dissolution and precipitation. This method, characterized by its simplicity and cost-effectiveness, typically involves plating baths containing fluoride, phosphate, carbonate, and chromate. Chromium layer coatings have been banned due to certain toxicity to the human body [99–102]. Pure Mg dissolves easily in HBSS (Hank's solution, pH 7.4) and almost disappears after a full day of immersion. Mass change of Mg (99.9 % in purity) in HBSS at 25 °C is given in Fig. 2, pure Mg treated with saturated $NaHCO_3$ solution has high corrosion resistance [58], depending on the treatment time. Over 3 h to 75 days of treatment, weight not only did not decrease, but increased, indicating new precipitation on the surface, as shown in Fig. 2(a). $NaHCO_3$ with a mass of 9 % and $Na_2CO_3$ aqueous solution with different pH values were treated at 25 °C for 20 h to investigate its corrosion resistance. When $NaHCO_3$ treated pH at 8.3, no corrosion was observed in HBSS for at least 20 days, and the results are shown in Fig. 2(a), almost the same as that in Fig. 2(b) (pH was 8.3). In addition, pure Mg, when treated in $NaHCO_3$ with the pH of 8.3, produced strong gas bubbling and a rise in pH (from 8.3 to 9.2 after 20 h treatment). Bicarbonate ion was a quite important factor to form protective layer and pH 8.3 gave the maximum fraction. The chemical reactions that should take place are as follow:

$$Mg + NaHCO_3 + H_2O \rightarrow MgCO_3 \downarrow + NaOH + H_2 \uparrow \quad (1)$$

The improvement of corrosion resistance is mainly due to the formation of $MgCO_3$ chemical conversion film, which inhibits further erosion.

#### 2.1.2. Hydrothermal treatment

Hydrothermal treatment involves the surface of Mg alloy acquiring adequate energy in a high-temperature and high-pressure environment, facilitated by a surfactant in a hydrothermal solution. In this process, Mg spontaneously combines with $OH^-$ in the hydrothermal treatment solution, existing in the form of $Mg^{2+}$, resulting in the precipitation of $MgOH_2$ on the matrix surface. This leads to the formation of a metal oxide film.

One instance of hydrothermal coatings involves creating superhydrophobic and highly adhesive coatings on pure Mg using a solution that incorporates sodium oleate (SO) [80]. In the course of hydrothermal treatment, oleate groups bind to the surface of the layered double hydroxide (LDH)/SO coating in two distinct manners, as illustrated in Fig. 3(a). LDHs consist of positively charged brucoid layers and interlaminar regions containing various anionic and solvated molecules [82–84,103]. SO is a low surface energy material with good biocompatibility and is often used as a surfactant [85,86]. Oleate groups selectively adhere to the $Mg(OH)_2$ crystal through van der Waals force and hydrogen bonding [81]. Concurrently, the electrostatic attraction between the positively charged metal hydroxide layer of Mg–Al LDH and the negatively charged oleate groups facilitates the binding of a substantial quantity of oleate groups to the surface of the LDH/SO sample. Fig. 3(b and c) illustrates the state of contact of the drip with the LDH or LDH/SO sample. The superhydrophobic nature of the surface is attributed to the combination of nanosheet-like features and the presence of hydrophobic long-chain aliphatic oleate groups [86]. The robust adhesion is a result of the collaborative effects between the negative pressure induced by the volume alteration of the sealed air pocket and van der Waals attraction at the solid-liquid interface [87,104].

By single-step hydrothermal treatment, a highly crystalline Hydroxyapatite (HAp) coating was formed on pure Mg using

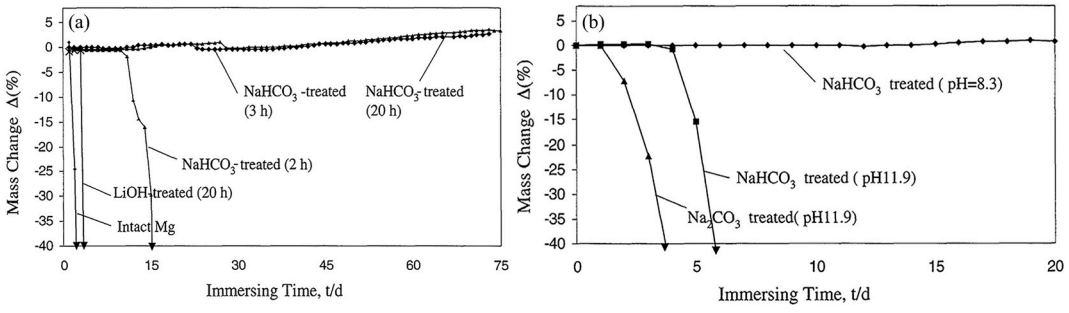


**Fig. 2.** Mass change of Mg in HBSS at 25 °C: **(a)** aqueous saturated $NaHCO_3$ and 0.01 kmol/$m^3$ LiOH was used at 25 °C, **(b)** test specimens were treated with 9 mass% of $NaHCO_3$ and $Na_2CO_3$ for 20 h at 25 °C [58].

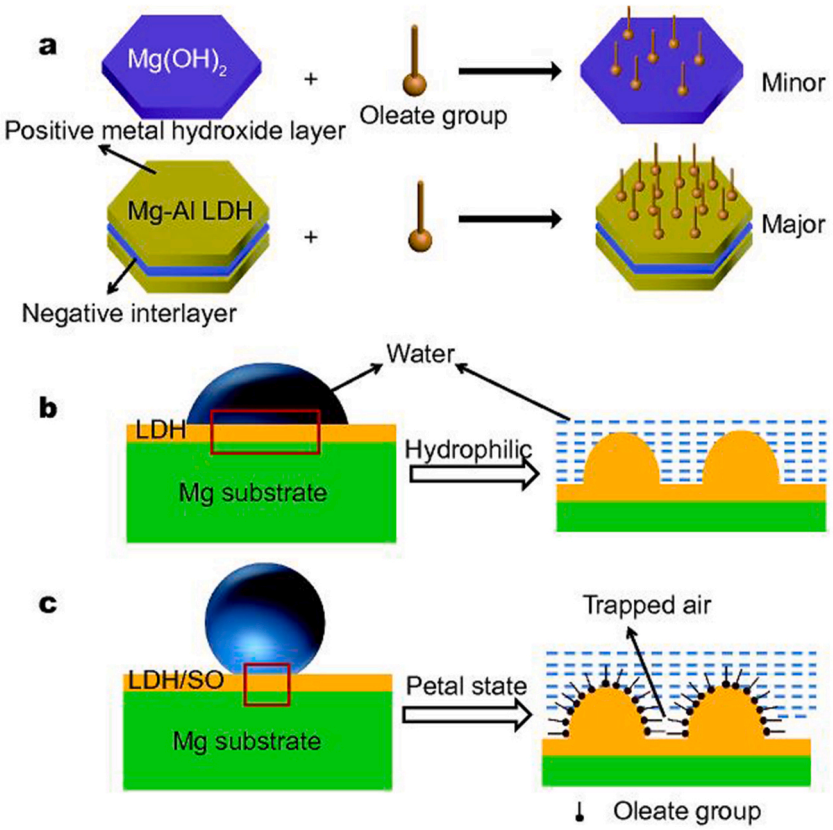


**Fig. 3.** depicts the following: **(a)** Schematic representation illustrating the binding of oleate groups on $Mg(OH)_2$ and Mg–Al LDH, **(b, c)** Schematic representation illustrating the interaction of water with the surfaces of LDH and LDH/SO samples [80].

$C_{10}H_{12}CaN_2Na_2O_8$ solutions at different pH values [105]. The morphology of the HAp coating exhibited variations corresponding to changes in pH values. HAp possesses stable chemical properties within the body and constitutes a key component of bone structure. The application of an HAp coating significantly enhanced the corrosion resistance of pure Mg, surpassing a tenfold improvement. HAp coating defects were sealed intact by precipitated HAp during the 4-day immersion process. HAp coating prevents localized corrosion. And with the extension of processing time, the protective performance of HAp coating is improved. By combining fluoride treatment and hydrothermal treatment, a Ca-deficientca-deficient hydroxyapatite (CDHA)/$MgF_2$ bi-layer coating prepared on high-purity Mg had strong adhesion strength and corrosion resistance [106]. In vitro cell experiments showed that MG63 cells had significant improvements in adhesion, proliferation and differentiation on pure Mg with CDHA/$MgF_2$ bi-layer coating.

The coating derived from the hydrothermal treatment process exhibits a robust bond with the matrix, and adjustments to the coating's thickness and morphology are achievable by controlling hydrothermal time and pH values. This, in turn, allows for the modulation of the material's degradation rate. However, a drawback of the hydrothermal treatment process is its susceptibility to destruction by chloride ions ($Cl^-$), limiting its ability to offer prolonged protection to the substrate. Current research in the medical pure Mg field is focusing on enhancing the corrosion resistance and biocompatibility of hydrothermal coatings by introducing the Layered Double Hydroxide (LDH) structure, where $Mg(OH)_2$ serves as the primary component. Further investigations are necessary to elucidate the corrosion resistance mechanism and long-term biological effects of LDH coatings.

### *2.1.3. Alkali-heat treatment*

Alkali-heat treatment is usually used as a pre-treatment to obtain a coating with some corrosion resistance, and sometimes it is also used as an intermediate layer to strengthen the adhesion between the substrate and the outer layer. Alkali-heat treatment is one of the steps in removing oil and impurities from Mg and Mg alloys.

Pure Mg underwent treatment with a 5.0 M NaOH aqueous solution at 60 °C for 36 h, resulting in the generation of numerous passivating hydroxyl (-OH) groups on the Mg surface, as illustrated in Fig. 4(a) [88]. Then, the dried Mg–OH samples were washed with 0.02 M ascorbic acid (AA) for 24 h in ethanol at 37 °C. Treatment of Mg–OH with AA can induce adequate chemical bond bonding by –OH and –COOH bonds, thus forming a protective layer. Following this, the Mg substrate treated with AA was immersed in a 0.5 mM bovine serum albumin (BSA) solution for 48 h at 37 °C. BSA establishes robust bonds via $–NH_2$ groups and hydrogen bonding. This characteristic renders Mg–OH-AA-BSA an excellent contender for a highly biocompatible, protective nanoscale layer structure that markedly improves corrosion resistance. The electrochemical corrosion results of Mg–OH-AA-BSA is given in Fig. 4(b). The

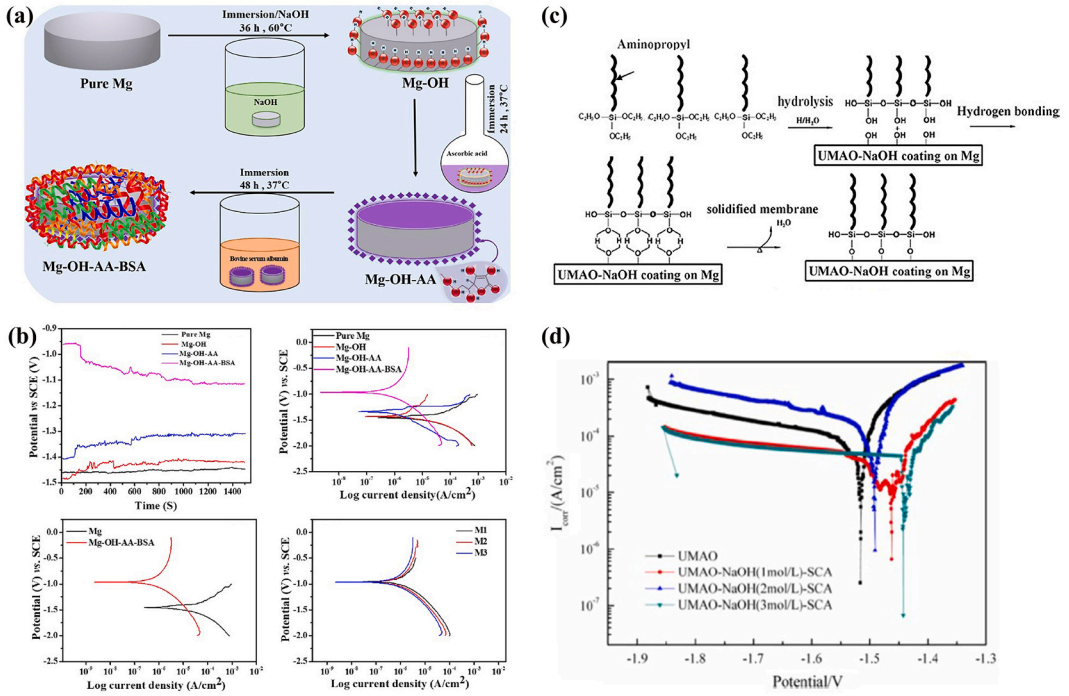


**Fig. 4.** Schematic diagrams of alkali-heat treatment on pure Mg surface and its corresponding electrochemical corrosion results: **(a)** an illustrative depiction showcasing the modification of the pure Mg surface through a layer-by-layer formation of chemical bonds, resulting in the assembly of Mg–OH-AA-BSA. This modification aims to enhance both anti-corrosion properties and osteo-inductive characteristics, **(b)** electrochemical corrosion results of Mg–OH-AA-BSA [88], **(c)** a schematic representation detailing the processing mechanism of UMAO-SCA treatment and **(d)** tafel polarization curves illustrating the electrochemical behavior of Mg plates subjected to various treatments [73].

UMAO-treated samples underwent an alkalization process by immersion in NaOH solutions of varying concentrations (1 mol/L, 2 mol/L, 3 mol/L) and subsequent heating at 60 °C for 1 h. Following this, the samples were rinsed with clean water and allowed to dry. Subsequently, the alkalized samples were immersed in a silicon coupling agent (SCA) and heated to facilitate the formation of the final cured film. The utilized SCA, aminopropyl triethoxysilane ($NH_2(CH_2)_3Si(OC_2H_5)_3$), consists of aminopropyl and ethoxy groups. In the hydrolysis process, the -*Si*-$OC_2H_5$ group undergoes hydrolysis to generate -*Si*-OH. These silanols are adsorbed on the substrate, and dehydration condensation between the -*Si*-OH groups leads to the formation of -*Si*-*O*-Si bonds. Additionally, Si–OH groups combine with –OH on the substrate surface to establish hydrogen bonds. The heat-curing process involves dehydration reactions, resulting in the formation of covalent bonds (-*Si*-*O*-Mg) with the substrate. At the interface, one silicon hydroxyl from the silane reacts with the surface of the base material, while the remaining two -*Si*-OH groups either condense with other -*Si*-OH groups in different silanes or remain in a free state. This process is illustrated in Fig. 4(c) [73]. The alkaline cleaner on the Mg surface can retain a large amount of basic hydroxyl groups, which provides more attachment points for the deposition of silane membranes, making Si–*O*–Mg binding stronger. The results showed that the diameter of the holes formed on the surface after UMAO treatment decreased with the increase of NaOH concentration (1 mol/L, 2 mol/L, 3 mol/L). Compared with the single UMAO treatment, the corrosion potential ($E_{corr}$) of the Mg substrate treated by alkali - heat treatment increased by 29 mV, 53 mV and 75 mV with the increase of NaOH concentration, respectively, which are shown in Fig. 4(d), and the corrosion current density ($I_{corr}$) decreased by 1-2 orders of magnitude, indicating that the corrosion resistance of the coating after alkali - heat treatment and silicon treatment was improved.

In summary, the significant advantage of alkali - heat treatment technology on pure Mg surfaces is making the implant has better corrosion resistance and biocompatibility. The limitation is that the resulting coating is very thin, so it is usually only used to create an intermediate layer, which inevitably increases the technical difficulty and cost of surface treatment.

### *2.1.4. Anodic oxidation*

Anodizing is a technique wherein a corrosion-resistant oxide film is developed on the metal surface through the application of current in a specific electrolyte and under defined process conditions [74]. At the heart of this process lies the creation of an anodic oxide layer, typically 5–30 μm thick, characterized by its hardness, density, wear resistance, and electrical insulating properties. The surface's pore size and distribution depend on factors such as electrolyte properties, temperature, anodizing current density, and voltage. Recognizing anodic oxidation as one of the most effective anti-corrosion technologies for Mg alloys, numerous fundamental studies have been conducted, leading to the continuous development of new anodizing technologies [74–77].

Some studies in earlier years gave similar results and confirmed the conclusion [74,78,79,107] that in 1 M NaOH, when the voltage was 3 V, the current density remained low, forming a light gray $Mg(OH)_2$ protective film. In the voltage range of 3–20 V, a thick black

$Mg(OH)_2$ film was formed. At voltages exceeding 20 V, a thin protective coating was once again formed. The breakdown phenomenon caused by dense discharge (above 50 V) limited the formation of compact anodic film [108]. Controlled precipitation of calcium phosphate on Mg can be achieved through a combination of anodizing and autoclaving [76]. In 1 M NaOH, different anode voltages can form a rough and smooth anodic oxide film. The amount of calcium phosphate precipitation on porous membranes was 2–3 times higher than on smooth membranes. Autoclaving does not notably alter the topography of the anodized film; instead, it restricts the precipitation of calcium phosphate. The surface of the pure Mg plate was further treated by anodizing to generate a HA coating [77]. In the HA-Mg group, no gas formation or plate exposure was observed until week 12, whereas the Bare-Mg group exhibited consistent gas formation and plate exposure starting from week 2. The HA-Mg group demonstrated a statistically significant superiority in terms of degradation resistance compared to the Bare-Mg group.

The anodized coating is an insulator, unlike some existing intermetallic hard coatings: the intermetallic hard coating is cathodic to the Mg substrate, and if the coating breaks down somewhere, it will expedite the corrosion deterioration of the substrate. In addition to good adhesion with the matrix, the anodized coating also has high thermal stability, thermal shock resistance, heat resistance and high dielectric strength, which provides greater performance improvement space for the application of Mg alloy.

### *2.1.5. Plasma electaolyte oxidation*

PEO, also known as micro-arc oxidation (MAO), relies on precise adjustments of electrolyte and electrolytic parameters. This process, occurring under instantaneous high temperature and pressure generated by arc discharge, fosters the growth of modified porous structure ceramic-like coatings on the surface of Mg and Mg alloys. These coatings primarily consist of matrix metal oxides complemented by electrolyte components. Notably, PEO exhibits significantly improved anti-corrosion and wear resistance performance compared to traditional anodized coatings, making it a focal point of interest in the medical Mg alloys domain [41,60–65]. PEO treatment on 99.9 % pure Mg metal, utilizing a mixed electrolyte comprising sodium silicate, sodium fluoride, calcium hydroxide, and sodium hydroxide, resulted in the formation of a porous oxide layer with high roughness [66]. Increasing the voltage of the PEO treatment in the C1 electrolyte from 200 V to 250 V, led to a substantial decrease in the hole area, reducing it from 21 % to 9 % (refer to Fig. 5(a)). Additionally, PEO treatment in the C2 electrolyte yielded the creation of wells with an average diameter ranging from 1 to 5 μm, with some individual wells reaching up to 25.0 μm. The pore area of C2 coatings varied from 15 % (at 250 V) to 12 % (at 300 V) (see Fig. 5(a)). Pore size plays a crucial role in cell adhesion and proliferation, with data indicating that pore sizes within the range of 5–70 μm are conducive to osteoblast adhesion and proliferation. The introduction of $Ca(OH)_2$ into the electrolyte led to a reduction in contact angle values (see Fig. 5(b)). C2 300V exhibited the lowest contact angle (0°), indicating a highly hydrophilic surface. This outcome suggested that the presence of $Ca^{2+}$ contributed to the growth of the oxide layer, resulting in a more active surface area. Cell culture experiments corroborated these findings, demonstrating favorable adhesion in samples treated with $Ca(OH)_2$ containing electrolytes and a consequential significant increase in cell proliferation rates. MAO-coated samples are not cytotoxic during in vivo degradation and are able to form more new bone around them [67,69,70]. MAO-coated pure Mg has good cytocompatibility and biocompatibility.

PEO coatings demonstrate outstanding resistance to both wear and corrosion [68]. Additionally, the phase composition of the coating can be controlled through electrolyte composition adjustments. However, the presence of micropores and cracks in the film layer, resulting from arc-flash discharge, may negatively impact the long-term corrosion resistance of coatings [60]. Building upon the current technology for PEO coatings on Mg alloys, the preparation of multi-stage composite coatings to fill holes of PEO is an important

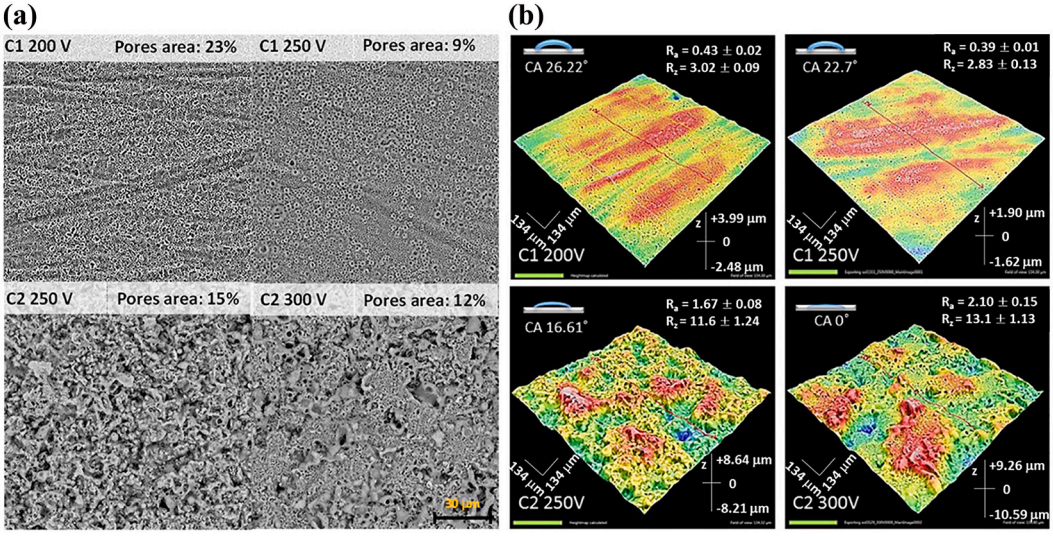


**Fig. 5.** (a) displays the SEM image illustrating the surface of pure Mg samples post-PEO process, highlighting the pore area, **(b)** 3D topographical maps of pure Mg samples are presented, along with details on surface roughness and contact angle (CA) parameters of the coatings [66].

research direction of surface modification of pure Mg and Mg alloy [61–63].

The surface modification of the pure Mg mesh involved a combination of PEO and hydrothermal treatments, resulting in the creation of a compact protective layer primarily consisting of $Mg(OH)_2$ and amorphous calcium phosphate on the Mg substrate [64]. Results showed that the rate of biodegradation of Mg mesh was not only significantly delayed, but also that the surface modification of Mg improved bone volume and bone density in skull defects compared to the original Mg mesh. In order to seal the pores in the silicate-based PEO layer on the surface of pure Mg, the two-step spin coating method was used to coat the polylactic acid (PLLA) on the PEO coating, which was very beneficial to improve the local degradation performance of the bearer implant [71]. The alloy coated with PEO-PLLA exhibited no localized degradation even after 100 h of exposure to SBF, whereas the Mg coated solely with PEO displayed signs of local degradation after 48 h. Additionally, the impact of berberine on the coating characteristics of ultrasonic MAO/polylactic acid and glycolic acid copolymer/berberine (UMAO/PLGA/BR) was investigated [72]. Different amounts of BR have different degrees of sealing effect on the corrosion channel. At a butyric acid (BR) content of 3.0 g/L, the UMAN/PLGA/BR coating exhibited the lowest self-corrosion current density at $3.14 \times 10^{-8}$ A/cm$^2$, signifying enhanced corrosion resistance. The UMAO/PLGA/BR coating demonstrated remarkable biological activity, effectively addressing the challenges of rapid degradation and susceptibility to infection associated with pure Mg in clinical settings. The application of KH550 silane coupling agent (SCA) on the UMAO-coated pure Mg was crucial for this improvement [73]. In comparison to sole UMAO treatment, the corrosion potential ($E_{corr}$) of pure Mg treated with UMAO-NaOH-SCA increased by 29 mV, 53 mV, and 75 mV, respectively. Simultaneously, the corrosion current density ($I_{corr}$) exhibited a reduction of 1-2 orders of magnitude, indicative of the enhanced corrosion resistance of the coating following silicon treatment.

At a butyric acid (BR) content of 3.0 g/L, the UMAN/PLGA/BR coating exhibited the lowest self-corrosion current density at $3.14 \times 10^{-8}$ A/cm$^2$, signifying enhanced corrosion resistance. The UMAO/PLGA/BR coating demonstrated remarkable biological activity, effectively addressing the challenges of rapid degradation and susceptibility to infection associated with pure Mg in clinical settings. The application of KH550 silane coupling agent (SCA) on the UMAO-coated pure Mg was crucial for this improvement [73].

PEO offers significant advantages by effectively enhancing corrosion resistance, wear resistance, and biocompatibility, while maintaining non-toxic properties [99]. Notably, the porous surface morphology of PEO serves a dual purpose: it positively influences the adhesion of surface coatings and cell adhesion, while simultaneously acting as a potential source of fatigue cracks and entry points

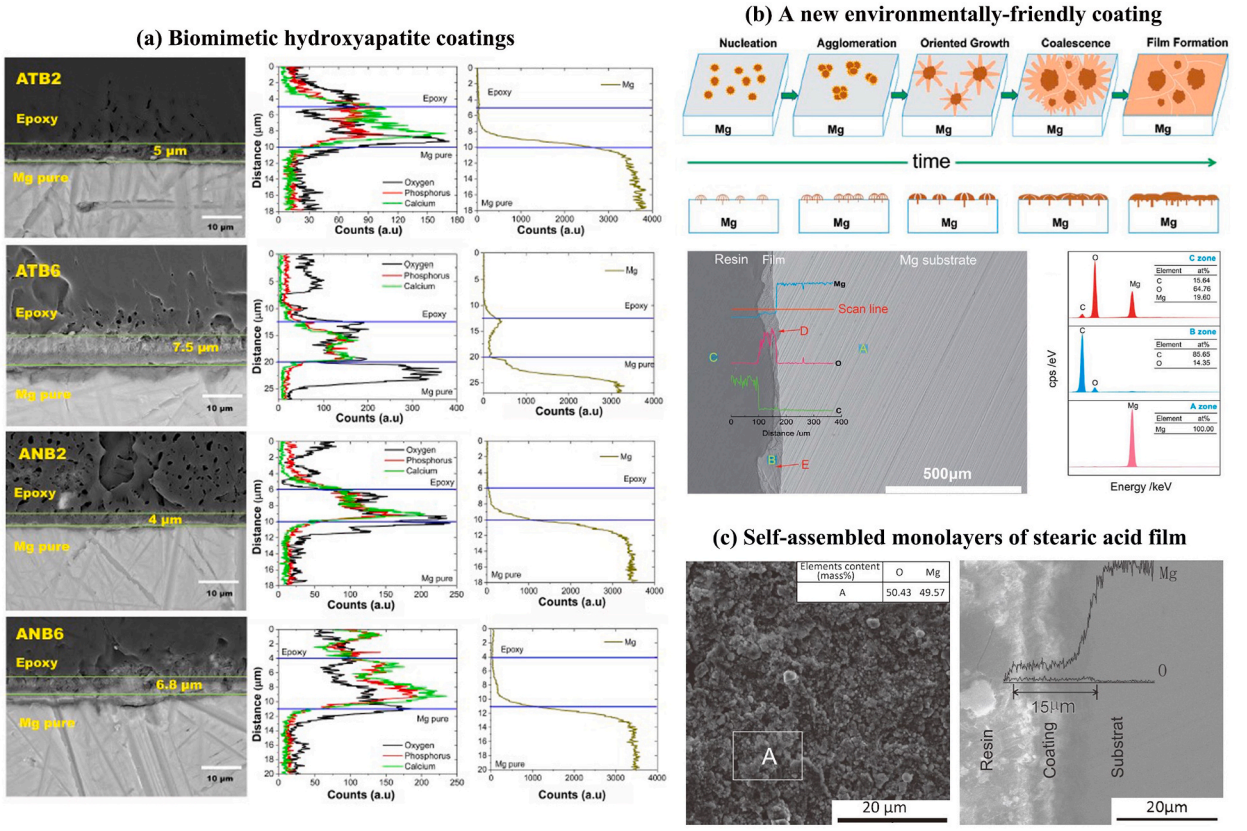


**Fig. 6.** SEM analysis of various advanced coatings formed on pure Mg: **(a)** SEM micrographs and corresponding linear cross-section EDS analysis profiles showcasing the HAp-coated samples in cross-sectional view [109], **(b)** proposed formation mechanism of nesquehonite film on the pure Mg substrate and cross-sectional observations of samples [111], and **(c)** SEM micrographs depicting the surface morphology, along with the corresponding EDS results, of SAMs of SA film [112].

for corrosive media.

#### 2.1.6. Advanced coating technologies

In recent years, for the surface modification of pure Mg, in addition to the above series of relatively traditional chemical treatment methods, it also includes a variety of composite coating preparation methods, biomimetic deposition technology and some environmentally-friendly coating preparation methods that have received widespread attention, see e.g., Fig. 6(a) [109]. Bioactive HAp coatings were applied to the pure Mg surface, resulting in HAp and/or doped apatite coatings with varying characteristics based on different preparation parameters. The thickness of the HAp coating was determined using SEM, and the cross-sectional micrograph and linear composition profile were analyzed through EDS. Throughout the HAp coating thickness, the concentration of P remains constant. However, at the Mg/HAp coating interface, the concentration of Ca and O is higher. The concentration of Mg is lowest at the coating edge and increases near the HAp/Mg interface. Tomozawa and Hiromoto [110] reported the preparation of HAp bilayers using a solution with a pH of 5.9. In this study, a comparable pH value was employed. Under conditions of relatively low temperature and high humidity, a protective film of nesquehonite ($MgCO_3{\cdot}3H_2O$) was spontaneously formed on the surface of pure Mg samples through an in-situ reaction between the Mg surface and $CO_2$ in the medium-pressure gas phase. The formation mechanism is illustrated in Fig. 6 (b) [111]. This carbonation method is simple and green, involves only $CO_2$ and water, and the $CO_2$ gas and the resulting solution can be easily recycled. Pure Mg was heated in 773 K air for 10 h to form a MgO layer on its surface, and then a composite coating of self-assembled monolayers (SAMs) was formed after soaking in ethanol solution with a certain concentration of Stearic Acid (SA) for several hours, and the cross-sectional morphology and composition are shown in Fig. 6(c) [112]. This experiment revealed two crucial conclusions: (1) without the presence of deionized water, there was no noticeable development of a protective film on the surface of pure Mg; (2) despite the evacuation of air in the autoclave using $N_2$ flow for 4 h, the formation of the protective film still took place. These observations indicate that, although oxygen is not obligatory, the existence of water is crucial for the formation of the protective film. Based on all the experimental results mentioned above, the reactions possibly involved in the formation of $MgCO_3{\cdot}3H_2O$ were deduced:

when encountering water molecules adsorbed on the pure Mg surface, $CO_2$ is hydrated to form $H_2CO_3$ [113]:

$$CO_2 + H_2O + H_2CO_3 \tag{2}$$

that then dissociates in a two-step process described by:

$$H_2CO_3 \leftrightarrow H^+ + HCO_3^- \tag{3}$$

$$HCO_3^- \leftrightarrow H^+ + CO_3^{2-} \tag{4}$$

according to both methods, localized electrochemical reactions occurred on the Mg surface, including hydrogen evolution reactions and the electrochemical dissolution [55]:

$$Mg \rightarrow Mg^+ + e^- \tag{5}$$

$$2Mg^+ + 2H^+ \rightarrow Mg^{2+} + H_2\uparrow \tag{6}$$

or

$$2H^+ + 2e^+ \rightarrow H_2\uparrow \tag{7}$$

$$\mathrm{Mg} \rightarrow Mg^{2+} + 2e^- \tag{8}$$

then, the $Mg^+$ and $CO_3^{2-}$ ions combine to form $MgCO_3{\cdot}3H_2O$ crystal nuclei according to:

$$Mg^{2+} + CO_3^{2-} + 3H_2O \rightarrow MgCO_3 \bullet 3H_2O \tag{9}$$

as reactions 2–9 progressed, the formation of $MgCO_3$ nuclei increased, leading to the emergence of high-density nucleation sites. Following this, during the initial phases of film development, the Mg substrate underwent a gradual overlay of minute crystalline particles. As the reaction time extended, these grains continued growing, largely uninterrupted, until they approached one another. Upon contact, the horizontal expansion of two adjoining dendritic crystals halted, initiating a bonding process that ultimately led to the complete coverage of the entire Mg substrate surface with a continuous and dense $MgCO_3{\cdot}3H_2O$ film.

The advantage of these advanced coatings is that they can overcome the shortcomings of traditional single coatings such as limited corrosion resistance, poor adhesion, lack of biological activity and environmental hazard during the preparation process, which is the future development trend [73,109–112,114,115]. Among them, the degradation behavior of composite coatings is more complex, and the degradation rate cannot be calculated or predicted, so the behavior mechanism under in vitro and in vivo conditions needs to be further studied and verified. In addition, combining the advantages of each coating and developing functionalized composite coatings is also an important research direction for surface modification of pure Mg and Mg alloys in the future.

### 2.2. Physical methods

The typical methods of pure Mg surface physical modification can be summarized into two types, one is various mechanical

methods, and the other is physical vapor deposition method [99]. In these cases, the formation of surface-modified layers, thin films or coatings of pure Mg is mainly due to heat, kinetic energy and electrical energy rather than chemical reactions [116].

Friction stir processing (FSP) is a widely employed and effective advanced manufacturing technique that employs frictional heat and plastic deformation to enhance the surface characteristics of pure Mg in its solid state. Derived from friction stir welding (FSW), FSP operates on the fundamental principle of heating the tool to the material's plastic deformation temperature through the friction stir head. This process induces a plastic deformation zone on the material's surface, leading to effects such as grain refinement, nanoification, and material strengthening. Consequently, these modifications contribute to an overall improvement in the material's performance [117–120].

Physical vapor deposition (PVD) involves the creation of a thin film through the process of evaporating or sputtering a material within a vacuum environment. This results in the deposition of the material onto the substrate's surface. Specifically, the principle of PVD is to place the material target in a vacuum chamber and apply an energy source such as a heat source or electron beam to cause the target to produce atoms, molecules or ions evaporation or sputtering. These evaporated or sputtered substances are transported to the surface of the substrate, where the atoms in the surface lattice condense and react, eventually forming a homogeneous film. In the PVD process, commonly used energy sources are resistance heating, electron beams, laser or vacuum discharge. These energy sources can provide enough energy to allow the atoms, molecules, or ions in the target to gain enough kinetic energy to overcome the adsorption energy on the surface to reach the substrate surface and deposit to form a thin film. In addition, in order to guarantee the quality of the film, PVD needs to be carried out in a vacuum environment to avoid interference and contamination by impurities [121–123].

In the biomedical field, the surface properties of materials are critical, including aspects such as corrosion resistance and mechanical compatibility. In recent years, thin-film metallic glasses (TFMGs) coatings have been shown to significantly improve the performance of materials [124–129]. PVD methods, such as sputtering and pulsed laser deposition (PLD), are effective manufacturing techniques for the preparation of such thin films [126]. These findings have important application potential in the biomedical field. Therefore, this module focuses on the method of obtaining TFMG with extraordinary properties using PVD.

### *2.2.1. Mechanical methods*

A prominent method for mechanically modifying the surface of pure Mg involves the application of Friction Stir Processing (FSP), an innovative solid-state processing technology derived from Friction Stir Welding (FSW) [89,130]. Fine-grained Mg-nano-hydroxyapatite (Mg-nHAp) composites were developed by dispersing nHAp particles into pure Mg using FSP. During FSP, a cylindrical rotating tool with small pins is inserted into the material's surface, inducing dynamic recrystallization through intense plastic deformation, resulting in a substantial refinement of grains [131]. The stirring action of the FSP tool is utilized to create metal matrix composites by incorporating secondary phase particles. Fig. 7(a) illustrates a typical photograph of the stirring zone in the FSP-Mg-nHAp sample. An optical macroscopic image obtained from the section of the FSP-Mg-nHAp specimen Fig. 7(b) illustrates the dimensions of a typical stirring zone, thermomechanical affected zone (TMAZ), and heat-affected zone (HAZ). The SEM images of the cross-section of the FSP-Mg-nHAp specimen reveal the distribution of nHAp near the surface (Fig. 7(c)) and the accumulation of additional nHAp beneath the surface (Fig. 7(e)). EDS analysis corresponding to white particles, shown in Fig. 7(c) and **(e)**, indicates the presence of calcium and phosphorus, which confirms nHAp incorporation into the matrix. In vitro bioactivity studies have shown that the hydrophilicity and biomineralization of the composites were significantly enhanced due to particle refinement and the presence of nHAp, respectively. Electrochemical assessments aimed at scrutinizing corrosion behavior unequivocally demonstrated an enhancement in corrosion resistance attributable to both grain refinement and augmented biomineralization.

Mechanical treatment modification method of pure Mg surface, in addition to the above FSP, the physical means of surface modification of some Mg alloys, Al alloys, Ti alloys and stainless steel also have certain reference value, such as surface mechanical

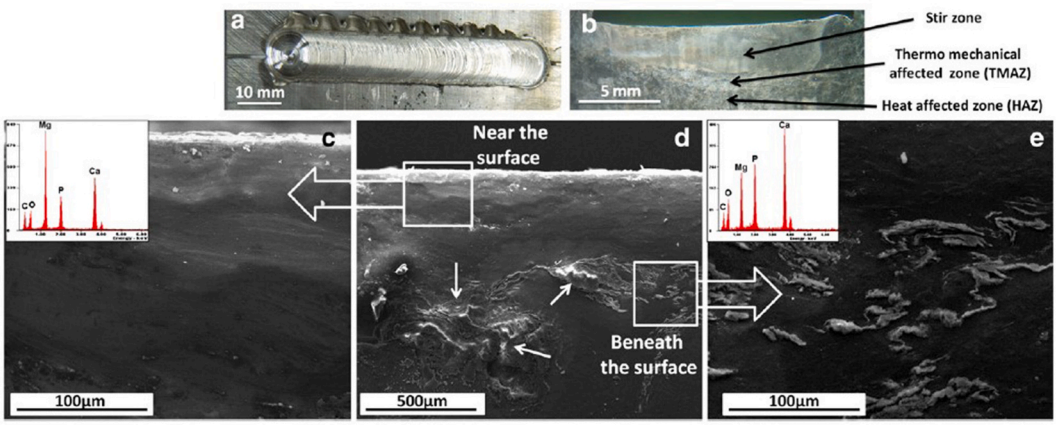


**Fig. 7.** (a) FSP - Mg - nHAp sample surface stirred zone, **(b)** FSP - Mg - nHAp sample cross-section, **(c)** SEM image of cross-section close to the FSP-Mg-nHAp sample surface in high magnification, **(d)** cross-section in low magnification, and **(e)** aggregated nHAp beneath the surface in high magnification [89].

attrition treatment (SMAT) [132–134], ultrasonic shot peening (USSP) [135,136], laser shock peening (LSP) [137], deep-rolling [138] and ultrasonic surface rolling process (USRP) [139,140] and other technologies, are the physical treatment, shaping or removal of the surface of the material [116]. In the context of USRP, significant plastic deformation occurs on the material's surface, leading to a notable enhancement in both mechanical properties and corrosion resistance. USRP stands out from other surface treatment technologies by offering a simultaneous improvement in surface properties, mechanical strength, and corrosion resistance. This multifaceted improvement aligns well with the primary objectives of mechanical modification, encompassing the attainment of specific surface topography and roughness, elimination of surface contaminants, and enhancement of adhesion for subsequent bonding processes.

### 2.2.2. *Preparation of TFMGs by PVD*

Materials can be broadly categorized into two groups: crystalline and amorphous. For crystalline materials, the arrangement of atoms is ordered and exhibits a certain degree of periodicity, characterized by a symmetric structure. In contrast, amorphous alloys have a disordered and random atomic arrangement, with a structure that is long-range disordered but short-range ordered. Amorphous alloys offer enhanced physical, chemical, and mechanical properties in comparison to crystalline alloys. These properties include heightened strength, wear resistance, and corrosion resistance, rendering them particularly appealing for diverse applications in electronics, aerospace, biomedical, and other industries [9,141].

Researchers have shown growing interest in Mg-based amorphous alloys owing to their combination of low weight, high specific strength, impressive mechanical characteristics, and notable corrosion resistance and hydrogen storage capacity. Currently, developed Mg-based amorphous alloys include Mg–Cu–Y, Mg–Ni–Y, Mg–Cu-Gd, as well as those that are promising for biomedical applications such as the Mg–Al–Zn, Mg–Ca, Mg–Zn, Mg–Zn–Mn systems, and the Mg–Zn–Ca system. Among these, Mg–Zn–Ca amorphous alloys, with their high specific strength (250–300 MPa $cm^3/g$) and excellent biocompatibility, are considered one of the most promising biodegradable implant materials [126,142,143].

The preparation of bulk metallic glasses (BMGs) with large volumes is challenging and typically limited to thin films with a thickness of 10 mm or less, which hinders their further application and commercialization due to the difficulty in achieving complex shapes. Rapid cooling (critical cooling rate) is the cooling rate at which molten liquid or melt can be solidified without causing crystallization. This rate is inversely proportional to the square of the sample thickness and directly proportional to the sample's thermal diffusivity [144]. The critical cooling rate ranges from 150 K/s to 1 K/s or lower, depending on the typical value of thermal diffusivity ($\kappa$) [145]. Therefore, thermal diffusivity and material thickness are crucial factors in obtaining a homogeneous metallic glass. Using TFMGs for surface modification of crystalline biological materials is a simple and reliable method because the phase

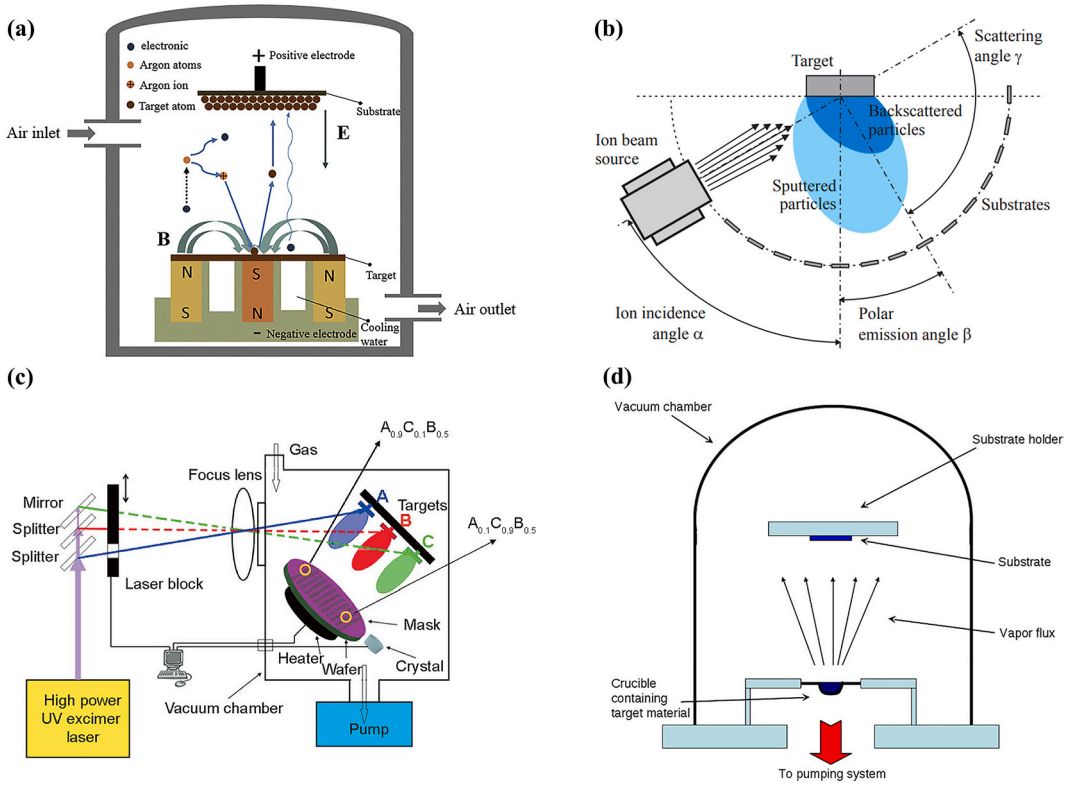


**Fig. 8.** Various PVD technologies: schematic of the **(a)** MS deposition system [147], **(b)** IBS deposition setup [150], **(c)** MPPLD system [156], and **(d)** thermal evaporation deposition system [158].

formed in TFMGs is amorphous, and their composition not only closely approximates that of BMGs [144], but also avoids the preparation barriers associated with BMGs, ultimately achieving the properties of metallic glasses. In the field of biomedical engineering, surface properties are of utmost importance, and the coating of TFMGs can significantly improve the mechanical compatibility and corrosion resistance of materials [146]. PVD is the most advantageous method for preparing such films.

PVD is a common thin film deposition technique that utilizes physical principles in a high vacuum environment to convert solid materials into gas-phase species, which are subsequently deposited onto substrate surfaces to form thin films. PVD techniques encompass a variety of methods including magnetron sputtering (MS), ion beam sputtering (IBS), pulsed laser deposition (PLD), thermal evaporation deposition (TED), etc.

Among these techniques, MS and IBS are the most commonly used methods with distinct principles. MS is a process that utilizes charged particles to bombard the target surface and eject materials to form thin films. In MS, a magnetic field is applied in a vacuum chamber to ionize the target surface, generating positively charged ions. These ions are then accelerated and implanted onto the target surface to cause sputtering, resulting in atoms leaving the surface and depositing onto the substrate. Therefore, MS is a technique that employs ionized gas to bombard the material surface (Fig. 8(a)) [147–149]. IBS, on the other hand, is a process that uses ion beams to bombard the target surface and eject materials to form thin films. In IBS, ion beams are accelerated and focused in a vacuum chamber, and then implanted onto the target surface to cause sputtering, resulting in atoms leaving the surface and depositing onto the substrate. Therefore, IBS is a technique that employs accelerated ion beams to bombard the material surface (Fig. 8(b)) [150–153]. So, the main difference between the two principles lies in the type of particles used to bombard the material surface, with the former utilizing ionized gas and the latter employing accelerated ion beams.

PLD is a technology that utilizes the energy of pulsed laser pulses to ablate materials from the surface of a target and deposit them onto a substrate to form a thin film. The basic principle of PLD is to use the high-energy pulsed laser to ablate materials from the surface of the target, and then deposit the ablated materials onto the substrate to form a thin film. The advantages of PLD include the ability to maintain good consistency in composition and structure between the thin film and the target material, as well as the ability to prepare very thin films with high quality, high control, and high complexity [154,155]. Fig. 8(c) shows a system schematic of Multi-Plume Pulsed-Laser Deposition (MPPLD). The excimer laser (Lambda Physic LPX 210i) produces a high-energy UV laser beam with a wavelength of 248 nm. More details are given elsewhere [156]. Thermal evaporation was invented by Faraday in the 50s of the 19th century [157]. In this process, atoms and atomic groups or molecules are removed from a metal crucible containing some bulk material (target) by heating the crucible, or by electric current in the form of steam flux, Fig. 8(d) is a schematic diagram of the evaporation system [158].

These methods are characterized by high efficiency, good reproducibility, fast deposition rates, high material conversion rates, and the ability to produce dense film structures. PVD techniques have been widely employed in various fields such as semiconductor,

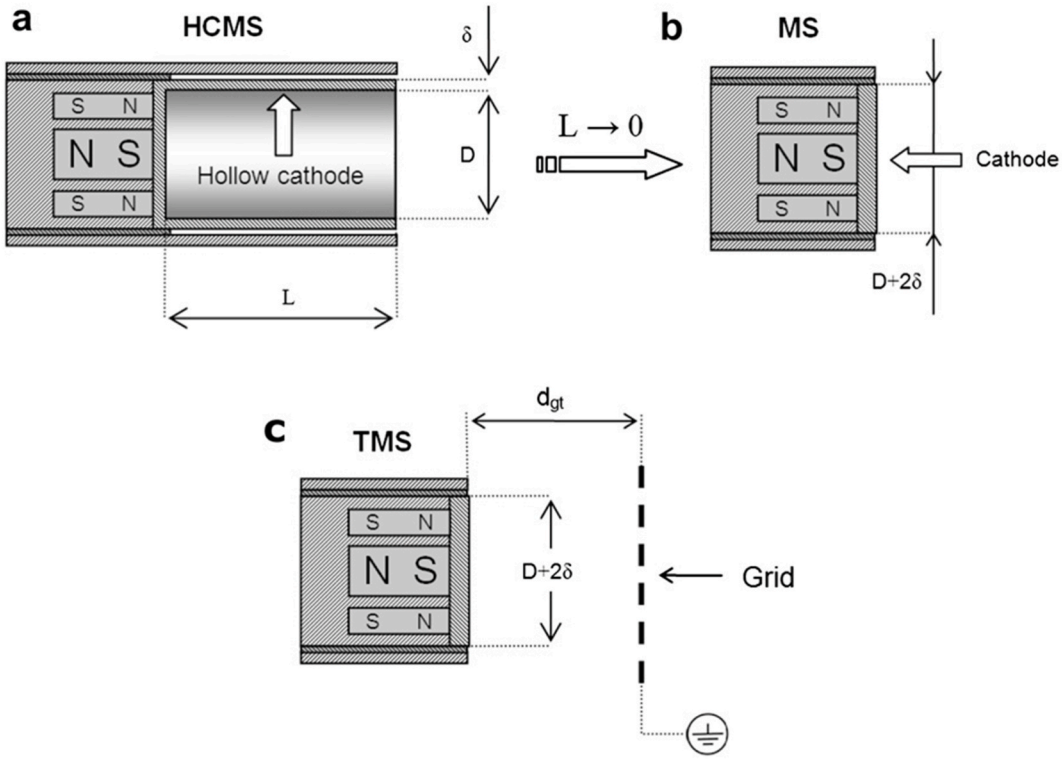


**Fig. 9.** Schematic cross-section of the cathodes used in the **(a)** HCMS, **(b)** MS and **(c)** TMS systems [168].

optoelectronics, chemistry, biomedical, and mechanical engineering for thin film fabrication and surface modification [118,124,159].

The preparation of TFMGs by PVD technology is one of the current research hotspots [160–163]. TFMGs are a class of amorphous metal materials with excellent properties such as high strength, high toughness, high wear resistance, excellent conductivity and chemical stability, and have a wide range of application prospects in engineering and scientific fields [126,164,165]. In the process of preparing TFMGs from PVD, the target material is sublimated into a gaseous substance under a high vacuum environment, and then deposited on the substrate surface to form a thin film [125,126,160,165,166]. By adjusting the PVD process parameters, such as deposition rate, temperature, pressure, atmosphere, etc., the structure and properties of TFMGs films can be accurately controlled, which provides new ideas and approaches for the large-scale preparation and application of TFMGs. Therefore, PVD technology has important application value and research significance in the preparation of TFMGs.

*2.2.2.1. Magnetron sputtering.* MS deposition has become the most widely used technique in metal and composite thin film deposition and is used in many industrial applications. MS technology has been evolving to improve target utilization, increase ionization of sputtered species, increase deposition rates, and minimize electrical instabilities such as arcs, as well as reduce operating costs [167]. This system operates on an unconventional glow discharge with magnetic confinement, achieved through strategically positioned magnets behind the cathode. This configuration creates an irregular magnetic field in front of the cathode (target), resulting in the magnetic entrapment of free electrons, compelling them to follow a spiral trajectory in the $\boldsymbol{E} \times \boldsymbol{B}$ direction. This confinement contributes to increased plasma density and elevated sputtering rates. The operational characteristics of the magnetron in this system can be elucidated by the following empirical laws:

$$I = KV^n \tag{10}$$

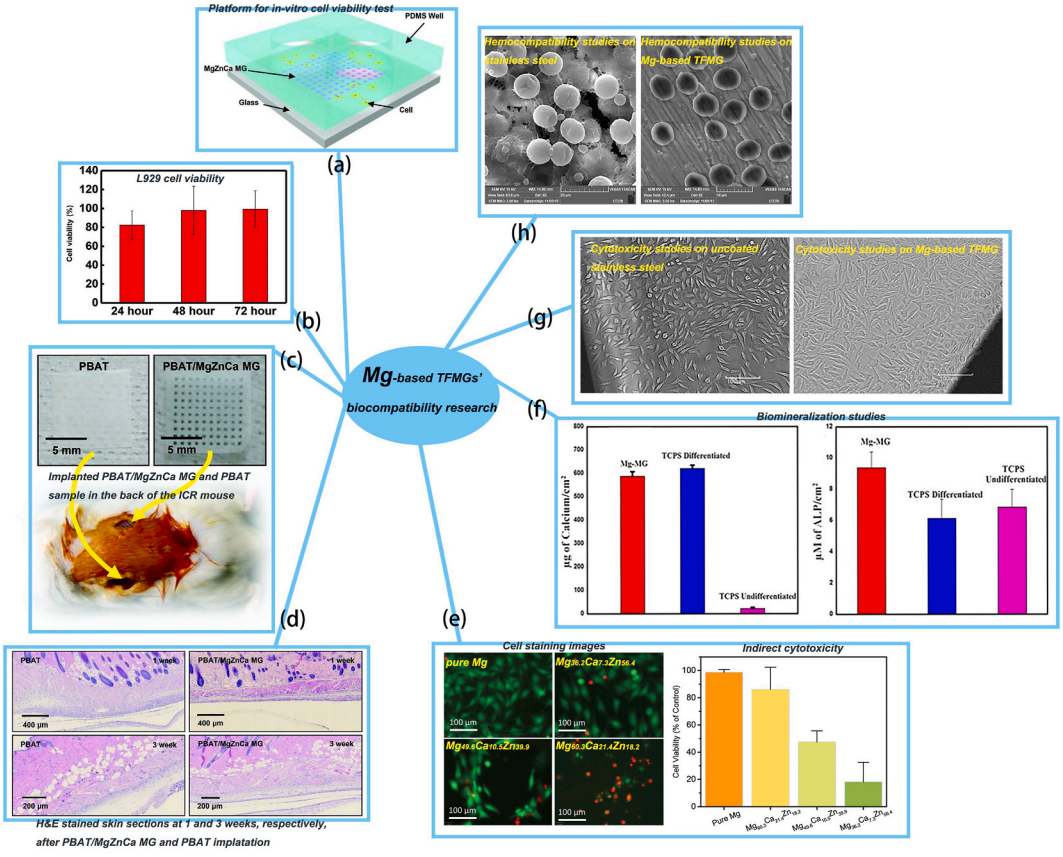


**Fig. 10.** Illustrative instances of biocompatibility research on Mg-based TFMGs include: **(a)** a schematic representation of the in-vitro cell viability test platform, where L929 cells are cultured on a glass substrate divided into a dot-patterned MgZnCa TFMG array (10 μm × 10 μm × 500 nm) and a bare glass surface, facilitating initial adhesion for cells in a custom-made PDMS chamber (8 mm diameter), **(b)** assessment of L929 cell viability over 72 h, calculated based on the number of cells attached to the bare slide glass (control) compared to the MgZnCa TFMG, **(c)** an image depicting implanted PBAT/MgZnCa TFMG and PBAT sample in the back of the ICR mouse, **(d)** images of H&E stained skin sections at 1 and 3 weeks post-implantation of PBAT/MgZnCa TFMG and PBAT [169], **(e)** cell staining images captured using a 20X Zeiss fluorescent microscope for pure Mg, $Mg_{36.2}Ca_{7.3}Zn_{56.4}$, $Mg_{49.6}Ca_{10.5}Zn_{39.9}$, and $Mg_{60.3}Ca_{21.4}Zn_{18.2}$, along with an assessment of the indirect cytotoxicity of these samples based on their increasing Zn content [170], **(f)** biomineralization studies on calcium and ALP assay, **(g)** cytotoxicity studies on uncoated stainless steel and Mg-based TFMG, and **(h)** hemocompatibility studies on uncoated stainless steel and Mg-based TFMG [175]. Reproduced based on the cited studies.

where *k* and *n* are functions of working gas, target material, pressure, system geometry, strength, and magnetic field configuration. For a fixed cathode voltage, an increase in *n* results in a higher current, which improves plasma confinement and leads to higher plasma densities, thereby enhancing the discharge conductivity. The exponent *n* is related to the efficiency of electron capture in the magnetron (thus reducing electron loss rate) and is a measure of the steepness of the I - V curve. Although conventional MS systems are a widely used tool for thin film deposition, improvements can also be made by changing the geometry and electrode structure. Examples of these different systems include hollow cathode MS (HCMS) and triode MS (TMS) systems (Fig. 9). See Reference [168] for more details.

Mg-based TFMGs have garnered significant attention owing to their favorable biocompatibility, biodegradability, and mechanical properties [126]. In the literature currently available, the most used method for preparing Mg-based TFMGs (mostly Mg–Zn–Ca components) is MS [169–178]. Utilizing magnets to create a parallel magnetic field to the target, MS enables operation at reduced voltage and pressure. The introduction of a magnetic field proves advantageous by capturing both primary and secondary electrons, drawing them closer to the target. This improved proximity enhances ionization efficiency and the bombardment of ions on the target, providing enhanced control over the deposition of coatings [159,179,180]. A completely biodegradable MgZnCa TFMG was proposed by Jae-Young Bae [169], which exhibits advantages of an amorphous phase without crystalline defects. The MgZnCa TEMG demonstrates high elastic strain (approximately 2.6 % in nano-tensile testing) and enhanced ductility (approximately 115 % when combined with a serpentine geometry). The biocompatibility of the film was confirmed through in vitro cytotoxicity and in vivo inflammation tests, as shown in Fig. 10(a-d). Compared to the bare stainless steel substrate samples, when the thickness of the MgZnCa amorphous film increased to 6 mm, the corrosion current density decreased to 0.26 mA/cm$^2$. The corrosion potential of the coated samples increased to −0.10 and −0.07 V. Morphological analysis also revealed a reduced level of corrosion and increased presence of degradation products in the coated samples compared to the uncoated material [174]. It was found by Li et al. that there is a significant correlation between the zinc concentration in Mg–Ca–Zn TFMG prepared by MS and the corrosion current, which is advantageous for the passivation behavior of the thin films. However, a negative correlation was observed between the zinc content and cytotoxicity (Fig. 10(e)) [170]. It was found by Datye et al. that there is a strong correlation between the hardness of the Mg–Zn–Ca system and Zn content [173]. In addition to corrosion resistance and biocompatibility of the thin film, the mechanical performance compatibility with the substrate needs to be considered. Designing the surface grain of the substrate into a gradient structure can significantly reduce the hardness mismatch between the amorphous layer and the magnesium alloy substrate [171]. Elevated levels of ALP, an early biomarker, which is considered as an essential factor for bone mineralization, were observed on the Mg-based metallic glass coated specimens. No inhibitory effect of TFMG on ALP activity was observed during the osteogenic differentiation process, as depicted in Fig. 10(f-h) [175].

The film structure prepared by MS is significantly influenced by the deposition parameters and the zinc content in the target material. It is possible to fabricate films with a precipitate-containing polycrystalline microstructure, as well as films with a microstructure composed of polycrystalline supersaturated solid solution and amorphous structure. Furthermore, the corrosion performance of the alloy is strongly influenced by the microstructure and deposition conditions. The corrosion rate is significantly reduced when no precipitates are present in the crystalline Mg matrix. It can be further decreased during the transition from a crystalline to an amorphous film [176–178,181].

*2.2.2.2. Ion beam sputtering.* IBS deposition is a kind of PVD technique. In comparison to other PVD methods such as MS or thermal evaporation techniques, IBS offers greater flexibility in tailoring the properties of the secondary film-forming particles. This flexibility

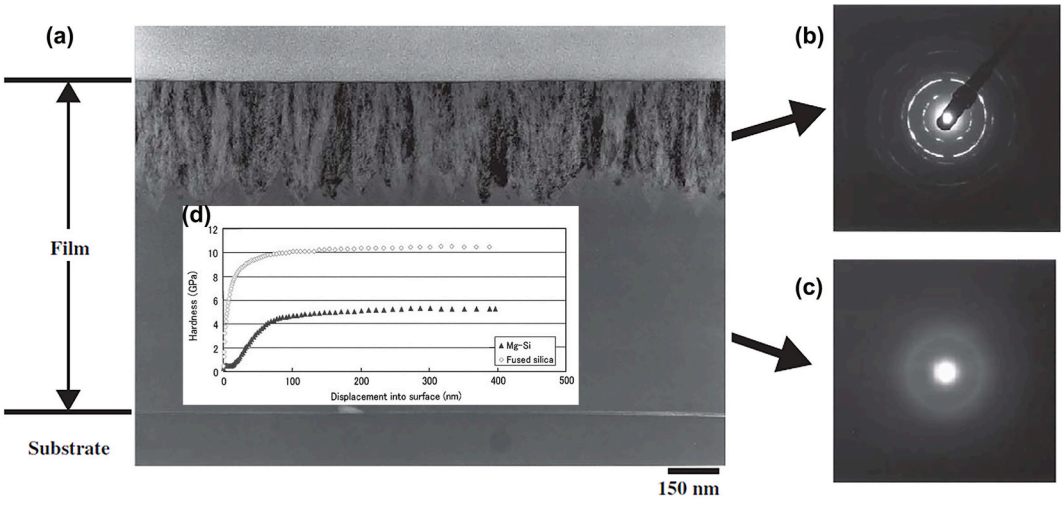


**Fig. 11.** The cross-section and mechanical properties of the film was deposited from the target of Mg/Si = 50 %: 50 % area ratio: **(a–c)** photographs of cross-sectional and electron diffraction patterns for upper and bottom layers in film, **(d)** mechanical properties of hardness [183].

allows for the fine-tuning of thin film characteristics. The IBS method was employed to grow amorphous $SiO_2$ thin films on a silicon substrate in an active oxygen atmosphere. These films were characterized by a substantial population of primary inert gas nanoparticles. The growth rate of the films was observed to increase with the higher ion energy and greater ion incidence angle [150,182]. The key distinction of IBS from traditional MS lies in the fact that, in conventional glow discharge sputtering systems, the substrate is directly exposed to the plasma environment, whereas IBS allow for a separation between the target material and the substrate, thereby shielding the thin films from thermal effects and radiation damage induced by the plasma. Researchers have utilized the IBS to deposit a bilayered $Mg_2Si$ thin film structure near room temperature, as depicted in Fig. 11. The upper layer consists of a crystalline columnar $Mg_2Si$ structure, while the lower layer is amorphous in nature. It is noteworthy that the mechanical properties, specifically the hardness, of the amorphous lower layer are significantly higher compared to the crystalline upper layer [183]. An amorphous thin film of $Mg_{1.2}Ni_{1.0}$ with a thickness of approximately 600 nm was prepared using IBS. Under conditions of approximately 150 °C and 3.3 MPa of $H_2$, the amorphous film exhibited a reversible hydrogenation-dehydrogenation reaction [184]. In comparison to cast alloys, these films exhibited superior corrosion behavior, characterized by higher polarization resistance and larger passive regions [185].

*2.2.2.3. Pulsed laser deposition.* PLD exhibits several distinctive features when compared to other thin film growth techniques. These include: (1) the ability to achieve near-stoichiometric composition of the target material in the deposited films; (2) flexibility and rapid response; (3) higher deposition rates; (4) lower synthesis temperatures and high orientation growth; (5) in-situ deposition of multilayer films; and, (6) ease of thickness control. While alternative deposition techniques are competitive for the fabrication of metallurgical films, PLD is versatile for depositing thin films of virtually any material, ranging from pure elements to multi-component alloys and compounds. A significant advantage of PLD lies in its capability to faithfully reproduce the chemical stoichiometry of the target material in the deposited films [186]. In recent years, PLD has found widespread applications in directing the ablated material plume from biocompatible ceramic targets onto substrate materials, creating thin biocompatible coatings suitable for dental or orthopedic implant applications. Specifically, PLD has been proven to be an effective method for the fabrication of crystalline thin films of HAp, which is a major mineral component of natural bone and one of the most widely recognized biocompatible materials [187–190]. To fully exploit the excellent biodegradability properties of Mg-based alloy films, it is imperative to conduct microstructural analysis of these films [191–197]. Unfortunately, there is limited literature reporting the use of PLD for the preparation of Mg-based alloy films. Furthermore, there remain several unresolved issues concerning the quality of films obtained via PLD, including issues such as solid target fragment or liquid cluster (droplet) ejection [198], which may result in the formation of various particles/precipitates on the deposited film surface [199]. Consequently, in order to obtain high-quality magnesium-based amorphous films, it is necessary to investigate the relationship between PLD process parameters and the microstructure of deposited films.

Sung Jae Chung et al. investigated the influence of process parameters and target composition on the microstructure of Mg–Zn–Ca TFMGs deposited using PLD. Their findings revealed that, when the substrate was cooled to −90 °C, the substrate temperature during deposition emerged as the primary parameter affecting the formation of TFMGs with a composition of $Mg_{60}Zn_{35}Ca_5$. It was also demonstrated that the microstructural characteristics of the deposited TFMG could be controlled by utilizing optimal deposition parameters [200]. S. Thanka Rajan et al. employed the PLD process to fabricate a Ti–Cu–Pd–Zr:B thin film system. Through XRD and TEM, the amorphous and disordered nature of the film was confirmed. Electrochemical experiments demonstrated that as the boron content increased, the film exhibited enhanced corrosion resistance and passivation ability, thereby preventing adverse biological reactions. The Ti–Cu–Pd–Zr:B coatings displayed excellent blood compatibility by suppressing platelet activation. Cellular morphology studies confirmed the viability of cells on the surface of the Ti–Cu–Pd–Zr:B TFMG. The results indicate that the Ti–Cu–Pd–Zr:B coatings with a boron concentration of 8 % (TiB-2) exhibit high corrosion resistance, hardness, and biocompatibility. Ti–Cu–Pd–Zr:B holds promising potential as a biomaterial for engineering implant applications [127]. The SEM micrograph of amorphous MG of $Zr_{59}Ti_3Cu_{20}Al_{10}Ni_8$ alloy coated on type 304L SS is shown in Fig. 12(a) [201], the SEM and TEM micrographs of Al–Mg–B–Ti films synthesized by femtosecond PVD is shown in Fig. 12(c and d) [202]. These results indicate that TFMGs deposited using PLD do not exhibit a smooth and flawless surface; instead, they feature dispersed particles of varying sizes distributed within the amorphous matrix. The presence of

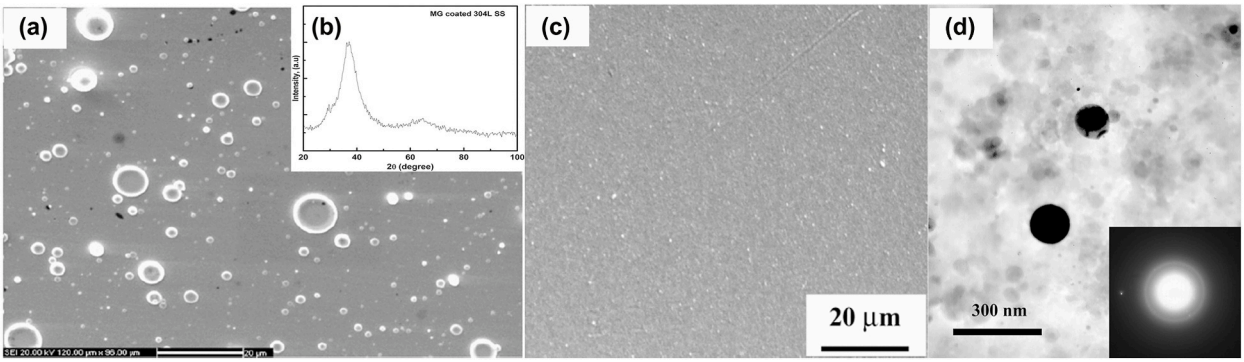


**Fig. 12.** SEM and TEM micrographs of amorphous metallic glass film surface by PLD: **(a)** SEM micrograph of MG of $Zr_{59}Ti_3Al_{10}Cu_{20}Ni_8$ alloy coated type 304L SS, **(b)** XRD pattern of amorphous MG of $Zr_{59}Ti_3Al_{10}Cu_{20}Ni_8$ alloy coated type 304L SS [201], **(c)** SEM micrographs of Al–Mg–B–Ti films synthesized by femtosecond PVD, **(d)** bright field TEM image of Al–Mg–B–Ti films synthesized by femtosecond PVD (plan view) [202].

these dispersed particles, characterized by a "doughnut" shape, is typically associated with the impact of molten droplets on the substrate surface during PLD. In contrast, the difference observed with the femtosecond PVD method is that it significantly reduces the particle density within the thin film, thereby lowering surface roughness.

Due to the unresolved issues in the performance of thin films obtained through PLD, such as the phenomenon of liquid clusters (droplets) that may lead to the formation of particles on the deposited film surface [198,199], and the limited literature on the preparation of Mg-based TFMGs using PLD, it becomes necessary to further investigate the relationship between PLD process parameters and the microstructure of deposited films in order to obtain high-quality Mg-based TFMGs.

*2.2.2.4. Thermal evaporation deposition.* Thermal evaporation, devised by Faraday in the 1850s, relies on the ability of a target material to evaporate at an appropriate temperature, where a substantial vapor pressure exists [157]. For most materials that evaporate below 1500 °C, this can be achieved by bringing the source material into contact with a heated surface, which is resistively heated by passing a current through it. Typical resistance heating elements include C, Mo, Ta, W, and BN/$TiB_2$ composite ceramics [203]. In essence, the principle of thermal evaporation exploits the fact that materials can evaporate at high temperatures, allowing for the deposition of the evaporated material onto a substrate through controlled heating. It is well-known that thermal evaporation was one of the earliest methods employed for obtaining amorphous materials. A key characteristic of this process is the requirement to maintain a relatively high vacuum level within the evaporation chamber. This is crucial because only under conditions of high vacuum can the evaporated molecules or atoms have sufficiently long mean free paths, enabling them to deposit onto the substrate's surface, resulting in high purity films [158].

Among the primary advantages of thermal evaporation, it is worth mentioning the high deposition rates, purity of the deposited films, relative process simplicity, and low equipment costs. However, thermal evaporation may not be well-suited for the fabrication of multi-component films due to differences in the melting points and vapor pressures of different materials. Additionally, the adhesion of films obtained through thermal evaporation to the substrate is often inferior to that achieved by MS.

Considering the functionality of screwing Mg bone nails into the body during surgical procedures, the adhesion between the thin film and the substrate becomes a critical aspect in the material preparation process. Based on the analysis of the characteristics of the evaporation method provided in the literature, it is evident that this method may not be the preferred choice for thin film preparation. The films produced using this method exhibit relatively weaker adhesion to the substrate compared to other approaches, which raises the possibility of film delamination during surgical procedures, compromising the quality of bone nails. However, it is precisely for this reason that this traditional method still holds value for further research. In the future, researchers in the medical field can shift their focus towards the study of the adhesion between the anticorrosive films prepared using the evaporation method and the substrate materials. This will open up a broader avenue for exploration, ultimately benefiting patients worldwide who require bone nail implants and whose needs align with these developments.

## 3. Mechanism of change of Mg implantation into bone

### 3.1. Pure Mg

The organic constituents responsible for constituting the human skeletal framework primarily encompass collagen proteins, fibers, and proteins, which bestow upon the bones their characteristic elasticity. The inorganic constituents comprising the human skeletal composition primarily include P and Ca, the role of which is to impart a requisite degree of hardness to the bones, thereby affording protection to vital organs, providing stabilization for muscles, and concurrently maintaining hematopoietic functionality. The human skeletal structure can be classified into two distinct categories based on its composition: cortical bone and cancellous bone, both sharing similar constituents but exhibiting significant disparities in terms of structure and strength, as depicted in Table 1 [204–209]. Cortical bone primarily resides in the long diaphysis and predominantly comprises mineralized tissue, with only minimal presence of bone marrow vasculature and connective tissue. It possesses a higher mass per unit volume and a lower porosity rate (10 %) compared to cancellous bone. Consequently, in contrast to cancellous bone, cortical bone demonstrates elevated tensile strength and elastic modulus, contributing to the overall skeletal strength. Cancellous bone, on the other hand, features a higher porosity level (50–90 %), facilitating a greater surface area for contact with red bone marrow and bone vasculature [210,211]. As a result, it exhibits a lower Young's modulus.

Mg is acknowledged as a crucial nutrient participating in diverse physiological processes and cellular metabolism in the human body. Its capacity to promote bone growth is attributed to the ability of Mg ions generated during degradation to stimulate the release of increased neurotransmitters, particularly calcitonin gene-related peptide (CGRP), from sensory nerve endings within the bone membrane. This, in turn, further facilitates the differentiation of mesenchymal stem cells into bone cells [212–215]. Fig. 13 illustrates a schematic representation of the mechanism through which $Mg^{2+}$ promote bone formation. These advantages underscore the suitability of Mg as an ideal material for bone fixation [215–218]. The ideal implant material in orthopedics should not only have a degradation

**Table 1**
Classification of bone and mechanical property parameters.

| Bone types | Porosity | Young's modulus (GPa) | Yield strength (MPa) | Tensile strength (MPa) | Ref. |
|---|---|---|---|---|---|
| Cortical bone | 10 % | 10–20 | 30–70 | 70–150 | [208,209] |
| Cancellous bone | 50%–90 % | 3–8 | – | – | [208] |

rate matching the healing speed of bone atissue but also induce mesenchymal stem cells to differentiate into osteoblasts or promote the growth of bone tissue cells effectively during the gradual degradation process. Simultaneously, its mechanical properties should match those of bone tissue to minimize the "stress shielding" effect and effectively aid and promote bone healing [210,219–222]. The primary purpose of implanting Mg into bones is to assist in bone injury healing rather than replacing human bones, as artificial materials cannot substitute for the functions of bone marrow, such as hematopoiesis and immunity. Fig. 14 illustrates a comparison of the Young's modulus among various materials and cortical bone [208,210]. From the figure, it can be observed that using pure Mg as a metallic material for orthopedic implants provides a better match with the elastic modulus of bone tissue. Additionally, the pure and harmless composition of Mg allows it to gradually degrade in the human body as bone healing progresses, producing harmless oxide by-products that are excreted through the kidneys and intestines, thereby avoiding stress shielding and the need for secondary surgeries.

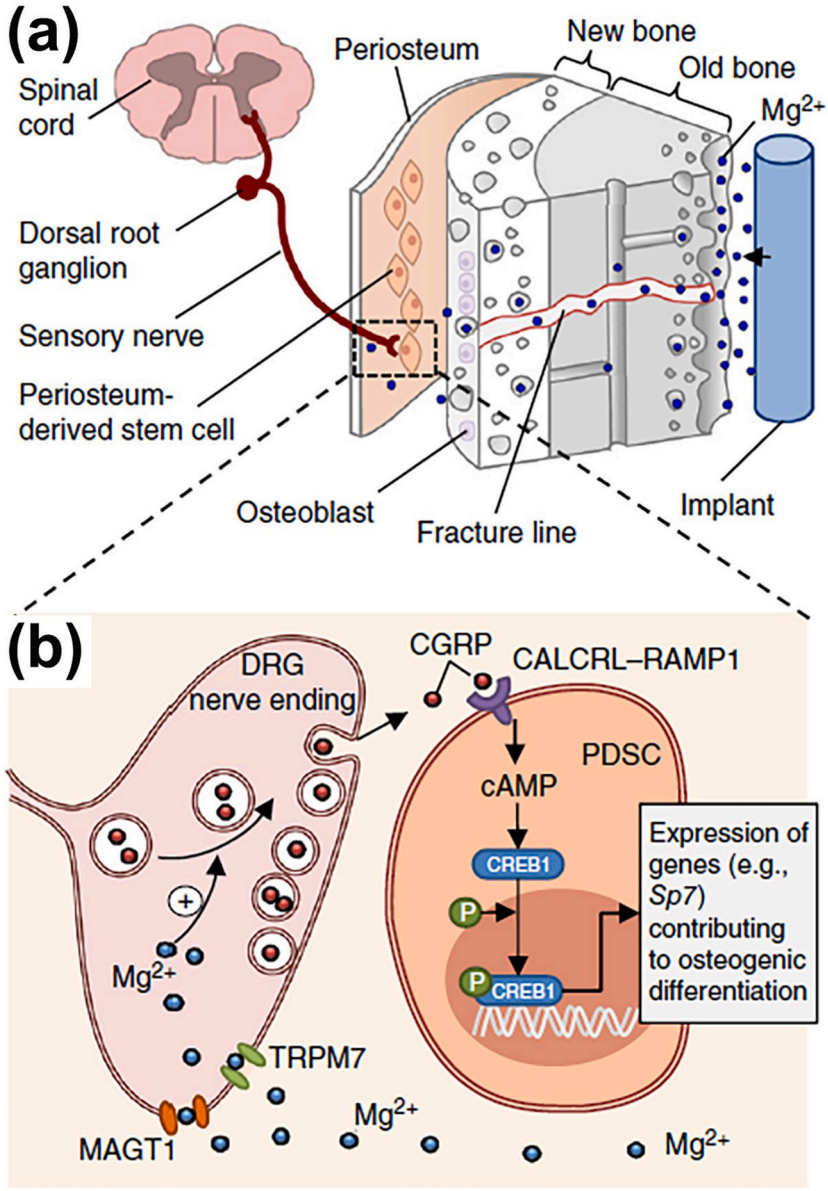


**Fig. 13.** A schematic representation of the mechanism through which $Mg^{2+}$ promote bone formation: **(a)** the diffusion of $Mg^{2+}$ derived from the implant across the bone towards the periosteum, which is innervated by DRG sensory neurons and enriched with PDSCs undergoing osteogenic differentiation into new bone, **(b)** released $Mg^{2+}$ enters DRG neurons via $Mg^{2+}$ transporters or channels (i.e., MAGT1 and TRPM7), promoting the accumulation and exocytosis of CGRP vesicles. The CGRP released by DRG then activates the CGRP receptor in PDSCs (consisting of CALCRL and RAMP1), triggering the phosphorylation of CREB1 via cAMP and promoting the expression of genes contributing to osteogenic differentiation [212].

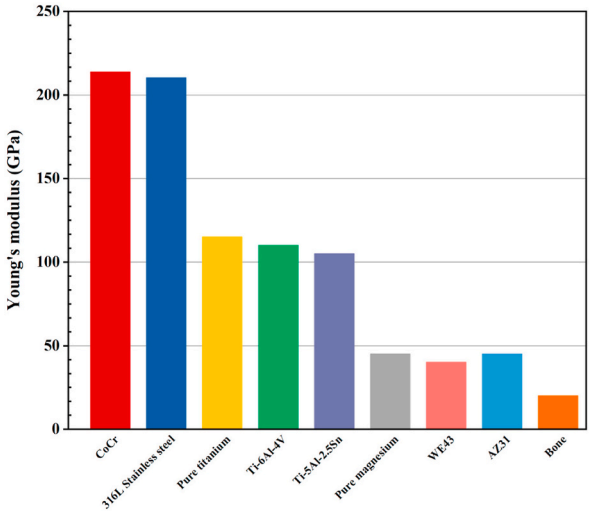


**Fig. 14.** Comparison of Young's modulus between different materials and cortical bone [208,210].

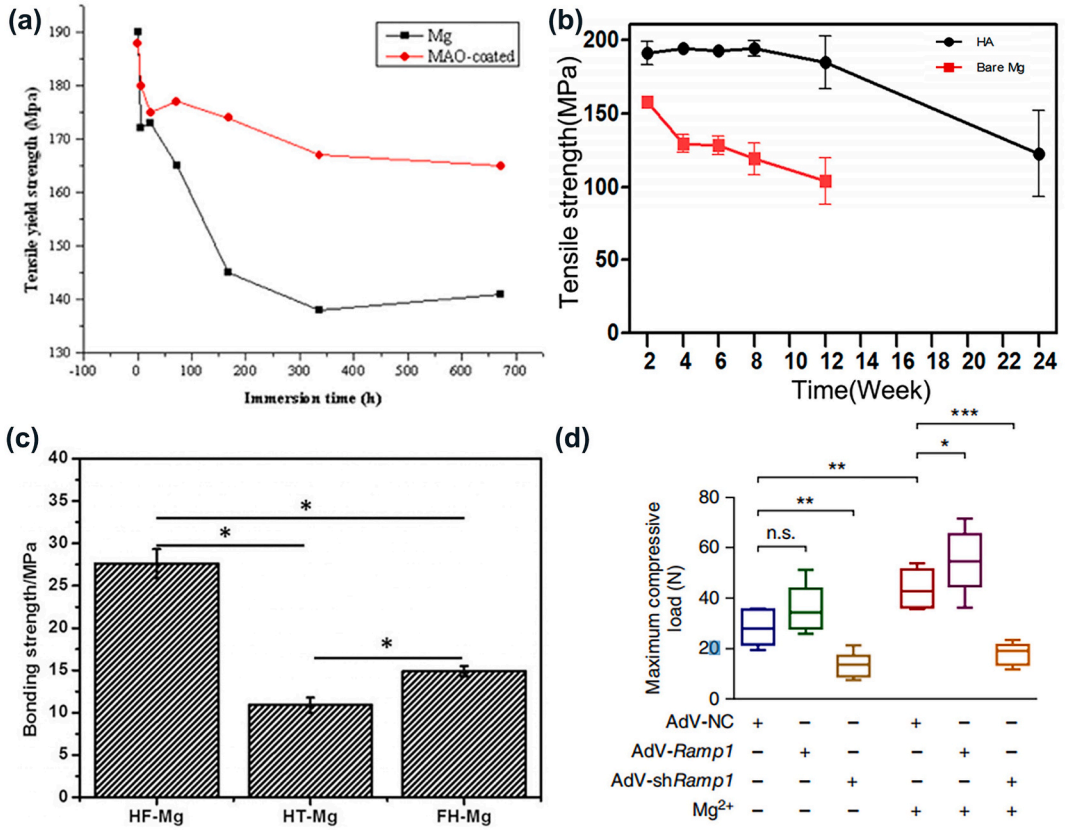


**Fig. 15.** Mechanical properties of pure Mg after surface modification: **(a)** tensile yield strength of the pure Mg and MAO-coated pure Mg over time [67], **(b)** tensile strength of the pure Mg and HA-coated pure Mg over time [77], **(c)** bonding strength between different coatings and Mg substrates, asterisks(*) indicate statistical significance, $p < 0.05$ [106], **(d)** and biomechanical test of maximum compressive load of the fractured rat femora 4 weeks after implantation with IMN or Mg-IMN in conjunction with treatment of AdV-NC, AdV-Ramp1 or AdV-shRamp1. n = 6 animals per group. *P < 0.05, **P < 0.01, ***P < 0.001, n.s., P > 0.05 by one-way ANOVA with Newman-Keuls post hoc test [212].

### 3.2. Pure Mg after surface modification

Pure Mg, renowned for its exceptional lightweight properties, has found widespread application in aerospace, automotive, and biomedical industries. However, its inherent limitations in terms of mechanical strength and corrosion resistance necessitate innovative strategies to enhance its overall performance. Surface modification emerges as a pivotal avenue in this pursuit. A myriad of surface modification techniques has been explored to augment the mechanical characteristics of pure Mg. Chemical treatments, coatings, and ion implantation represent prominent methodologies, each offering distinct advantages in tailoring the surface properties. The application of advanced coatings on the surface of pure Mg has demonstrated a marked improvement in its tensile strength. This augmentation is particularly noteworthy in applications where heightened tensile strength is imperative.

In Fig. 15(a), the influence of in vitro degradation on the tensile yield strength of two specimens is depicted. Tensile yield strength of both the MAO-coated and uncoated samples appeared comparable at the initial immersion point (i.e., time point 0). However, the strength of the uncoated specimens had experienced a rapid decline in the early stages of degradation, exhibiting a subsequently

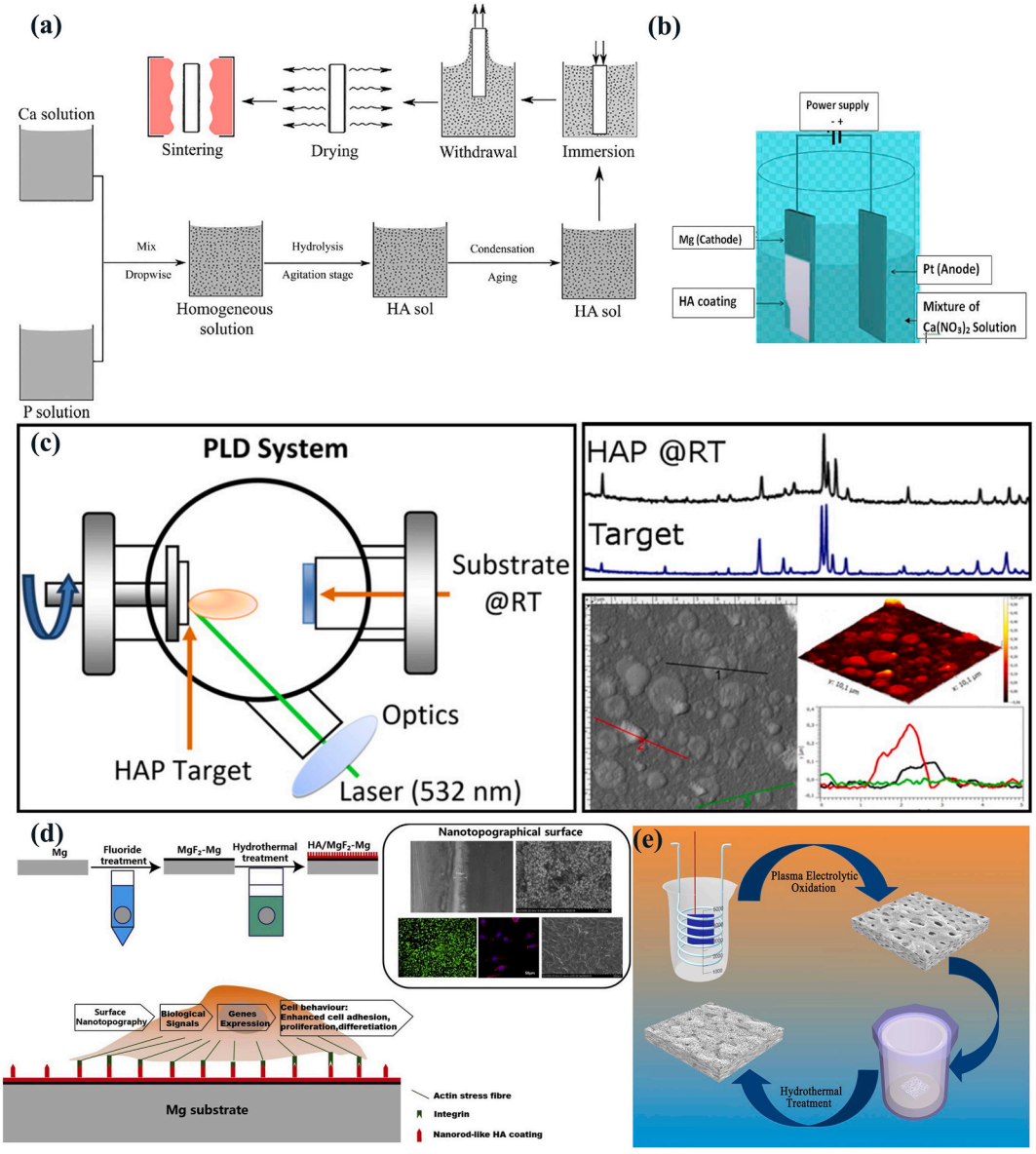


**Fig. 16.** Enhancing bone implant properties through coating processes: **(a)** key steps in the sol-gel preparation and application of HAp through dip and spin coating techniques [255], **(b)** process of electro - deposition for HAp coating [256], **(c)** process of Nd: YAG (532 nm) PLD technique for HAp coating [257], **(d)** combining fluorination and hydrothermal methods to fabricate CDHA/$MgF_2$ bilayer nano-coating on high-purity Mg surface [106], and **(e)** process of fabricating PEO/LDH coating [248].

attenuated rate of descent with increasing immersion time. This phenomenon may be attributed to the protective role played by corrosion products formed on the sample surface during the degradation process. Concurrently, the tensile yield strength of MAO-coated specimens remains virtually unaltered between the 6–30 day time interval. Following a 30-day immersion period, the tensile yield strength of the coated samples persists at approximately 165 MPa; conversely, the tensile yield strength of the uncoated samples diminishes to 140 MPa. Consequently, it is inferred that the MAO coating effectively contributes to the preservation of Mg's tensile yield strength over a specified duration [67]. The Mg plates with an HA coating maintained their tensile strength above 190 MPa for a duration of 12 weeks. In contrast, the bare Mg plates exhibited a rapid decline in tensile strength starting from the second week post-insertion ($p < 0.05$). Furthermore, as time progresses, there was a continual and significant decrease in strength ($p < 0.05$). The tensile strength of the test plates does not exceed 200 MPa, as evidenced by both Fig. 14 (b) [77]. In Fig. 15(c), the bonding strength of various coatings on the Mg substrate is presented. Specifically, the $MgF_2$ coating, CDHA coating, and CDHA/$MgF_2$ bi-layer coating exhibit bonding strengths of 27.64 ± 1.7 MPa, 10.90 ± 0.9 MPa, and 14.93 ± 0.6 MPa, respectively. The adhesion strength test results suggest that the presence of the $MgF_2$ interlayer enhances the bond strength between the CDHA coating and the Mg substrate, corroborating findings reported by Ren et al. [223], who employed $MgF_2$ as an intermediate layer between a CaP bioactive glass coating and Mg substrate, observing a significant augmentation in the bond strength between the bioactive glass coating and the Mg substrate. This improvement can be attributed to the $MgF_2$ interlayer's role in alleviating the disparities in hardness and thermal expansion coefficients between the HAp coating and the Mg substrate. By reducing the residual stresses between the HAp coating and the Mg substrate, the $MgF_2$ interlayer effectively enhances the bond strength [106]. Utilizing four-point bending biomechanical testing to ascertain the strength of fracture healing in different treatment groups, the results reveal that at the fourth week post-surgery, the maximum compressive load in the AdV-sh*Ramp1* treatment group with Mg-IMN implantation is significantly reduced compared to the AdV-NC treatment group. Conversely, the AdV-*Ramp1* treatment group with Mg-IMN implantation exhibits an elevated maximum compressive load [212] (see Fig. 16).

The surface modification of pure Mg stands as a transformative paradigm in tailoring its mechanical properties. The synergy of

**Table 2**
Reported electrochemical corrosion parameters of surface modified pure Mg.

| Coatings | Methods | Electrolyte | $E_{corr}$ (V) | $i_{corr}$ (μA/cm$^2$) | $R_p$ (kΩ cm$^{-2}$) | Ref. |
|---|---|---|---|---|---|---|
| Pure Mg | – | PBS | −1.54 | 22.2 | 58 | [80] |
| LDH | Hydrothermal treatment | | −1.47 | 14.4 | 79.8 | [80] |
| LDH/SO | | | −1.45 | 0.98 | 1160 | [80] |
| Pure Mg | UMAO + Chemical immersion | | −1.4781 | 24.019 | – | [98] |
| UMAO | | | −0.24934 | 1.5888 | – | [98] |
| UMAO@PTMC | | | −0.25737 | 0.42507 | – | [98] |
| UMAO@PTMC-PDA | | | −0.26185 | 0.58284 | – | [98] |
| Pure Mg | – | SBF | −1.93 | 331.0 | 6.9 | [106] |
| (CDHA)/$MgF_2$ bi - layer | Fluoride treatment + Hydrothermal treatment | | −1.45 | 2.24 | 819.0 | [106] |
| Pure Mg | – | | −1.46 | 10.42 | – | [88] |
| Mg - OH | Alkali - heat treatment | | −1.43 | 1.04 | – | [88] |
| Mg - OH - AA | Alkali - heat treatment + Chemical bonding | | −1.34 | 0.61 | – | [88] |
| Mg - OH - AA - BSA | | | −0.96 | 0.20 | – | [88] |
| UMAO | UMAO | 0.9 % | −1.517 | $2.135 \times 10^4$ | – | [73] |
| UMAO - NaOH (1 mol/L) - SCA | UMAO + Alkali - heat treatment + Silane treatment | NaCl solution | −1.488 | $2.73 \times 10^3$ | – | [73] |
| UMAO - NaOH (2 mol/L) - SCA | | | −1.464 | 892.7 | – | [73] |
| UMAO - NaOH (3 mol/L) - SCA | | | −1.442 | 238.3 | – | [73] |
| Pure Mg | – | HBSS | −1.80 | 32.0 | – | [70] |
| Ca - P | PEO | | −1.91 | 8.87 | – | [70] |
| Pure Mg | – | | −1.706 | 143.9 | – | [225] |
| Sr– CaP | Chemical immersion | | −1.549 | 5.208 | – | [225] |
| Pure Mg | – | SBF | −1.8 ± 0.02 | 23.5 ± 3.6 | – | [71] |
| MgO + $Mg_2SiO_4$ | PEO | | −1.92 ± 0.02 | 8.3 ± 3 | – | [71] |
| MgO + $Mg_2SiO_4$ + PLLA | PEO + Spin-Coating | | −1.54 ± 0.01 | 0.03 ± 0.2 | – | [71] |
| MgO + $Mg_2SiO_4$ | UMAO + PLGA + BR (3.0 g/L) | | −1.872 | (3.14 ± 0.017) × 10$^{-2}$ | – | [72] |
| Pure Mg | – | | −1.88 | 8705 | – | [89] |
| nHAp | FSP | | −1.57 | 674 | – | [89] |
| Pure Mg | – | 100 ppm NaCl solution, | −1.37 | 1.633 | – | [226] |
| Surface modification with hydrogen | EIR | pH = 12 | −1.249 | 0.296 | – | [226] |
| Surface modification with hydrogen | PIII | | −1.122 | 0.240 | – | [226] |

$E_{corr}$: corrosion potential, $i_{corr}$: corrosion current density, $R_p$: polarization resistance.

advanced techniques and the nuanced understanding of material behavior at the microscale offer unprecedented opportunities for optimizing pure Mg's performance in diverse applications. As we navigate the evolving landscape of surface modification technologies, the trajectory of pure Mg's utility is poised for a paradigm shift, promising enhanced mechanical robustness and extended applicability.

## 4. Biocorrosion of pure Mg after surface modification

During the service period within the human body, crystalline or non-crystalline Metallic implants continuously undergo the synergistic effects of corrosion and wear, leading to the release of alloying elements into the surrounding environment. This phenomenon triggers adverse effects such as toxicity, undesirable biological reactions, and site accumulation, ultimately resulting in implant failure. Not only does this process detrimentally impact the mechanical properties of the materials, but it also determines their biocompatibility [224]. Therefore, the design of biodegradable implant materials must encompass superior biocorrosion resistance to sustain the requisite mechanical integrity and effectively inhibit the release of metal ions induced by corrosion during the healing process. If, during the service life within the human body, the degradation rate of pure Mg can be attenuated to align with the growth rate of human skeletal tissue, deliberate enhancement of its mechanical properties becomes dispensable. This elucidates the rationale behind the deliberate consideration of both these facets in this review, as they are intimately interconnected. Consequently, for the clinical application of Mg, the foremost challenge to be addressed pertains to its suboptimal corrosion resistance.

Table 2 [70–73,80,88,89,98,106,225,226] presents corrosion data derived from Tafel curves obtained through electrochemical testing. These tests encompassed the use of PBS, SBF (simulated body fluid), HBSS (Hanks Balanced Salt Solution), and NaCl solution to simulate the human body environment. The biocorrosion behavior of surface-modified pure Mg was predominantly investigated through electrochemical experiments conducted in biological media. Electrochemical tests comprised techniques such as PDP (Potentiodynamic Polarization) and EIS (Electrochemical Impedance Spectroscopy). These rigorously conducted experimental methodologies contribute to a comprehensive understanding of the corrosion behavior of alloy materials in a biological environment and their potential impact on implants.

In comparison to pure Mg, LDH and LDH/SO samples prepared via hydrothermal treatment exhibit notably lower free current density ($i_{corr}$) and higher corrosion potential ($E_{corr}$). Particularly, the LDH/SO samples demonstrate a significant reduction in $i_{corr}$, while the polarization resistance ($R_p$) of LDH/SO samples is approximately 20 times that of Mg and LDH samples. These findings indicate the outstanding corrosion resistance of the LDH/SO coating. This outcome is attributed to the synergistic effect of air sealing, which reduces the corroded surface area, diminishes the presence of oleic acid groups on the surface, thereby inhibiting the transfer of electrons [80]. In recent years, synthetic polymers such as poly (lactic acid) (PLA), poly(1,3 - trimethylene carbonate) (PTMC), polyetherimide (PEI), and polymeric dopamine (PDA) have increasingly found application in the preparation of corrosion-resistant coatings [98,227–230]. The utilization of these polymers serves to diminish the permeation of aqueous solutions onto the surface of magnesium substrates, thereby conferring resistance to solution corrosion. The application of these polymer coating technologies marks significant advancements in the corrosion [18,231–234]. All components of the Mg-UMAO@PTMC-PDA corrosion-resistant composite coating exert influence on the biodegradation behavior of the Mg substrate. The inner layer's coarse MgO ceramic surface structure provides favorable conditions for the adhesion of PTMC. In contrast to the overall degradation patterns observed in PLA, poly (lactic-*co*-glycolic acid) (PLGA), or polycaprolactone (PCL), PTMC adheres to a sequential degradation pattern, contributing to a decelerated corrosion rate of the Mg-based material. Consequently, this composite coating effectively impedes the rapid degradation of Mg-based implants, preserving their integrity and mechanical properties during the initial stages of implantation [98]. The silane coupling agent (SCA) treatment of UMAO coatings effectively suppresses cathodic and anodic polarization reactions, providing Mg with an efficient protective mechanism and reducing its corrosion rate within the human body. Following SCA treatment of the UMAO film, the hydrolysis of silane molecules results in silanol, which reacts with the oxide and hydroxyl groups in the ceramic layer and undergoes dehydration to form a solidified film. This film acts as a barrier preventing the intrusion of corrosive media into the Mg, thereby elevating the corrosion potential [73]. The CDHA/$MgF_2$ bi - layer coatings effectively mitigates localized bone resorption induced by elevated pH. The enhanced corrosion resistance of FH-Mg stems, in part, from the increased binding strength between the CDHA and $MgF_2$ coatings. This arises due to the top layer of the CDHA coating exhibiting resilience against electrochemical degradation during experiments. Furthermore, even in the event of partial damage to the CDHA coating, the presence of the dense $MgF_2$ intermediate layer acts as an additional barrier, isolating the contact between SBF and the Mg substrate, thereby retarding the degradation of Mg [106]. While metal dissolution can be catalyzed by proteins [235], the presence of oxide and hydrate layers on the Mg surface actually strengthens the binding with BSA. Consequently, chemically modifying the Mg surface by establishing covalent bonds, amine bonds, and hydrogen bonds emerges as a reliable and enduring modification technique. The cathodic potential value of Mg–OH-AA-BSA is significantly elevated to −0.96 V, underscoring the effectiveness of this modification [88]. The improvement in corrosion resistance in FSP-Mg-nHAp was attributed to the rapid formation of a passivation layer and the reduction in electrochemical coupling strength between grain interiors and grain boundaries, a phenomenon that occurred as the grain size diminished during the sample preparation process [89,236,237].

The studies highlighted various strategies for enhancing the corrosion resistance of Mg-based materials in biomedical applications. Coatings such as CDHA/$MgF_2$ and UMAO films treated with SCA demonstrated significant improvements in corrosion resistance, attributed to the formation of effective passivation layers and the manipulation of grain size during sample preparation. Additionally, the utilization of polymers like PLA, PTMC, PEI, and PDA showcased promising results in corrosion protection. Future endeavors in this field could focus on optimizing the synergistic effects of these strategies, exploring novel coating combinations, and further elucidating the long-term performance of these corrosion-resistant materials in physiological environments. This collective research paves the way

for advancements in the development of robust and durable Mg-based implants, fostering their successful integration into clinical applications.

## 5. Outlooks

In the previous sections, we discussed in depth various methods for surface modification of pure Mg and alloys, with a focus on increasing its interest and application in the biomedical field. This module will start from the economic benefits, effects, advantages and disadvantages of pure Mg and alloys to look forward to the possible future directions.

The rationale behind the emphasis on documenting surface modification methods for pure Mg in this review lies in its distinctive mechanical properties akin to human bone and excellent biocompatibility when compared to most Mg alloys. The higher the purity of Mg, the better its corrosion resistance and mechanical performance. Currently, many scholars are addressing the challenge of rapid degradation and subsequent mechanical performance decline of Mg during its service in the human body by enhancing its properties through alloying [238–243]. However, alloying approaches may introduce additional components, leading to a reduction in biocompatibility. In the pursuit of stability and foundational principles, the author contends that implementing judicious corrosion prevention measures on the surfaces of high-purity pure Mg is one of the critical directions that must be further addressed in the future development of Mg implants. This assertion is grounded in the observation that, while the comprehensive mechanical properties of pure Mg closely resemble those of human bone, its corrosion resistance is comparatively deficient. Alternatively, one may state that in the context where the degradation rate of pure Mg implants in the body is relatively faster than the growth rate of bones, it is prudent to introduce elements beneficial to bone growth, such as Zn, Ca, P, through corrosion prevention treatments on the surface of pure Mg implants [244,245].

In the domain of surface modification of pure Mg, economic considerations are paramount. Current research indicates that methods such as hydrothermal processes and UMAO for modification are straightforward and exhibit relatively lower costs. In comparison to alternative approaches, these methods not only prove more economical but also excel in enhancing surface properties. Future developments, coupled with the realization of economies of scale, are expected to broaden the application of these methods in the surface modification of pure Mg. Surface modification profoundly impacts the biocompatibility and corrosion resistance of pure Mg. As gleaned from previous studies, materials of pure Mg employing techniques such as HAp [246], CDHA/$MgF_2$ [106,247] and PEO [248, 249] coatings exhibit outstanding performance in electrochemical processes. These methods effectively reduce corrosion rates and enhance biocompatibility, thereby opening new possibilities for the application of pure Mg in medical implants.

The formation of HAp coatings through calcium phosphate conversion on pure Mg and its alloys has been identified as a potential process to enhance Mg's corrosion resistance. However, research in this area remains limited. In the future, scholars need to conduct further investigations to validate the effectiveness of this technique. Several recommended directions are outlined.

1. Optimization of coating preparation parameters: further optimization of coating preparation parameters is necessary to enhance the efficacy of the technique.
2. In vivo studies in small animal models: in-depth in vivo studies in small animal models are essential to understand the long-term corrosion behavior through volume and weight analyses.
3. Long-term mechanical performance studies: long-term mechanical performance studies, such as stress corrosion and corrosion fatigue, are crucial for a comprehensive understanding of the coating's durability.
4 Addressing Identified Gaps: conducting further in-depth research to address identified gaps is paramount for improving the commercial viability of the coating process.

Additional research is required to confirm the effectiveness of hydroxyapatite coatings formed through calcium phosphate conversion on pure magnesium and its alloys. Scholars should focus on refining coating preparation parameters, conducting in vivo studies, and addressing long-term mechanical performance aspects to enhance the commercial feasibility of the coating process.

Of particular note is that, in comparison to crystalline coatings or films, non-crystalline films theoretically possess superior corrosion resistance and mechanical properties. Non-crystalline alloys, commonly referred to as metallic glasses, exhibit an internal atomic arrangement characterized by short-range order and long-range disorder [250–252]. Non-crystalline alloys have garnered significant attention due to their excellent physical and chemical properties, including high strength, high storing elasticity [253], and corrosion resistance [254]. With immense potential applications in defense, biology, medicine, military, construction, and other fields, non-crystalline alloys have become highly promising.

In the realm of medical implants, scholars have observed that elements Zn and Ca, when alloyed with Mg to produce MgZnCa-TFMGs, demonstrate a certain level of corrosion resistance and excellent biocompatibility [169–178]. Although the academic community has drawn some conclusions regarding the preparation methods and performance testing of MgZnCa-TFMGs, there remains a relative scarcity of in-depth research concerning degradable TFMGs and the interface characteristics formed with the substrate. Further investigation is needed to explore aspects such as in vitro antimicrobial properties, mechanical performance, compatibility with the parent material, and overall performance after implantation in living organisms.

## 6. Concluding remarks

In conclusion, this review delves into the realm of surface modification strategies for pure Mg and its alloys, especially pure Mg, with a primary focus on enhancing corrosion resistance and mechanical properties for potential applications in medical implants. The

intrinsic mechanical properties of pure Mg, akin to human bone, make it an attractive candidate, albeit hindered by its relatively poor corrosion resistance. Various surface modification techniques, including hydrothermal processes, plasma electaolyte oxidation, and other advanced coating technologies, have been explored to mitigate these challenges. The commercial feasibility of these surface modification processes is contingent on addressing identified gaps, optimizing coating parameters, and conducting thorough in vivo evaluations. The potential of pure Mg in biomedical applications is vast, and further exploration and refinement of surface modification techniques are imperative for unlocking their full potential.

In the grand tapestry of materials science and biomedical engineering, the pursuit of enhancing pure Mg's properties opens new frontiers, promising innovations that could revolutionize the landscape of medical implants. As researchers delve deeper into these intricacies, the future holds the promise of advanced materials that seamlessly integrate with the human body, ushering in an era of safer, more durable, and biocompatible medical implants.

## Data availability statement

This is a review article; therefore, no data available in the manuscript.

## CRediT authorship contribution statement

**Mengqi Gong:** Writing – review & editing, Software, Investigation, Data curation, Conceptualization. **Xiangjie Yang:** Supervision, Resources. **Zhengnan Li:** Formal analysis. **Anshan Yu:** Methodology. **Yong Liu:** Supervision. **Hongmin Guo:** Supervision. **Weirong Li:** Project administration. **Shengliang Xu:** Software. **Libing Xiao:** Software. **Tongyu Li:** Validation. **Weifeng Zou:** Software.

## Declaration of competing interest

The authors declare that they have no known competing financial interests or personal relationships that could have appeared to influence the work reported in this paper.

## Acknowledgement

This research received funding from the National Natural Science Foundation of China under Grant No. 51674144. The authors gratefully acknowledge the funding obtained school of advanced manufacturing, Nanchang University, Jiangxi Province, China. One of the authors Mengqi Gong thank Nanchang University, Nanchang, Jiangxi Province for providing her the doctoral assistantship and the research grant for this research.

## References

[1] F. Rupp, J. Geis-Gerstorfer, K.E. Geckeler, Dental implant materials: surface modification and interface phenomena, Adv. Mater. 8 (2010), https://doi.org/10.1002/adma.19960080316.
[2] O. Yigit, T. Gurgenc, B. Dikici, M. Kaseem, C. Boehlert, E. Arslan, Surface modification of pure Mg for enhanced biocompatibility and controlled biodegradation: a study on graphene oxide (GO)/Strontium apatite (SrAp) biocomposite coatings, Coatings 13 (2023), https://doi.org/10.3390/coatings13050890.
[3] W.S. Pietrzak, Principles of development and use of absorbable internal fixation, Tissue Eng. 6 (2000) 425–433, https://doi.org/10.1089/107632700418128.
[4] V. Biehl, T. Wack, S. Winter, U.T. Seyfert, J. Breme, Evaluation of the haemocompatibility of titanium based biomaterials, Biomol. Eng. (2002) 19, https://doi.org/10.1016/S1389-0344(02)00016-3.
[5] E. Kassab, A. Marquardt, L. Neelakantan, M. Frotscher, F. Schreiber, T. Gries, S. Jockenhoevel, J. Gomes, G. Eggeler, On the electropolishing of NiTi braided stents - challenges and solutions, Materialwiss. Werkstofftech. 45 (2014) 920–929, https://doi.org/10.1002/mawe.201400220.
[6] X. Li, S. Hao, B. Du, B. Feng, H. Li, P. Qiu, B. Huang, L. Cui, Y. Yang, High-performance self-expanding NiTi stents manufactured by laser powder bed fusion, Met. Mater. Int. 29 (2023) 1510–1521, https://doi.org/10.1007/s12540-022-01317-2.
[7] P. Jamshidi, C. Panwisawas, E. Langi, S.C. Cox, J. Feng, L. Zhao, M.M. Attallah, Development, characterisation, and modelling of processability of nitinol stents using laser powder bed fusion, J. Alloys Compd. 909 (2022), https://doi.org/10.1016/j.jallcom.2022.164681.
[8] S. Wang, Y. Zhang, Y. Qin, J. Lu, W. Liu, Improvement of TiN coating on comprehensive performance of NiTi alloy braided vascular stent, Ceram. Int. 49 (2023) 13405–13413, https://doi.org/10.1016/j.ceramint.2022.12.215.
[9] B. Zberg, P.J. Uggowitzer, J.F. Loeffler, MgZnCa glasses without clinically observable hydrogen evolution for biodegradable implants, Nat. Mater. 8 (2009) 887–891, https://doi.org/10.1038/NMAT2542.
[10] X. Li, X. Liu, S. Wu, K.W.K. Yeung, Y. Zheng, P.K. Chu, Design of magnesium alloys with controllable degradation for biomedical implants: from bulk to surface, Acta Biomater. 45 (2016) 2–30, https://doi.org/10.1016/j.actbio.2016.09.005.
[11] Y. Fu, S. Cui, D. Luo, Y. Liu, Novel inorganic nanomaterial-based therapy for bone tissue regeneration, Nanomaterials 11 (2021), https://doi.org/10.3390/nano11030789.
[12] W. Wang, G. Jia, Q. Wang, H. Huang, X. Li, H. Zeng, W. Ding, F. Witte, C. Zhang, W. Jia, G. Yuan, The in vitro and in vivo biological effects and osteogenic activity of novel biodegradable porous Mg alloy scaffolds, Mater. Des. 189 (2020), https://doi.org/10.1016/j.matdes.2020.108514.
[13] H.M. Mousa, D.H. Lee, C.H. Park, C.S. Kim, A novel simple strategy for in situ deposition of apatite layer on AZ31B magnesium alloy for bone tissue regeneration, Appl. Surf. Sci. 351 (2015) 55–65, https://doi.org/10.1016/j.apsusc.2015.05.099.
[14] P. Jiang, R. Hou, T. Chen, L. Bai, J. Li, S. Zhu, L. Wang, R. Willumeit-Roemer, S. Guan, Enhanced degradation performance and promoted bone regeneration of novel CaCO3-based hybrid coatings on magnesium alloy as bioresorbable orthopedic implants, Chem. Eng. J. 467 (2023), https://doi.org/10.1016/j.cej.2023.143460.
[15] K. Kumar, A. Das, S.B. Prasad, Recent developments in biodegradable magnesium matrix composites for orthopaedic applications: a review based on biodegradability, mechanical and biocompatibility perspective, in: 11th International Conference on Materials, Processing and Characterization (ICMPC), Indore, INDIA, 2020, pp. 2038–2042, https://doi.org/10.1016/j.matpr.2020.12.133.
[16] Y. Li, C. Wen, D. Mushahary, R. Sravanthi, N. Harishankar, G. Pande, P. Hodgson, Mg-Zr-Sr alloys as biodegradable implant materials, Acta Biomater. 8 (2012) 3177–3188, https://doi.org/10.1016/j.actbio.2012.04.028.

[17] M.R. Sahu, T.S.S. Kumar, U. Chakkingal, A review on recent advancements in biodegradable Mg-Ca alloys, J. Magnesium Alloys 10 (2022) 2094–2117, https://doi.org/10.1016/j.jma.2022.08.002.

[18] H. Khatun, M. Rahman, S. Mahmud, M.O. Ali, M. Akter, Current advancements of hybrid coating on Mg alloys for medical applications, Results Eng 18 (2023), https://doi.org/10.1016/j.rineng.2023.101162.

[19] W. Jin, G. Wu, A. Gao, H. Feng, X. Peng, P.K. Chu, Hafnium-implanted WE43 magnesium alloy for enhanced corrosion protection and biocompatibility, Surf. Coat. Technol. 306 (2016) 11–15, https://doi.org/10.1016/j.surfcoat.2016.02.055.

[20] F. Saconi, G.H. Diaz, A.C. Vieira, M.L. Ribeiro, Experimental characterization and numerical modeling of the corrosion effect on the mechanical properties of the biodegradable magnesium alloy WE43 for orthopedic applications, Materials 15 (2022), https://doi.org/10.3390/ma15207164.

[21] J. Kubasek, D. Dvorsky, M. Cavojsky, D. Vojtech, N.a. Beronska, M. Fousova, Superior properties of Mg-4Y-3RE-Zr alloy prepared by powder metallurgy, J. Mater. Sci. Technol. 33 (2017) 652–660, https://doi.org/10.1016/j.jmst.2016.09.019.

[22] L. Li, F. Qi, Z. Zhang, L. Lu, X. Ouyang, Corrosion, mechanical and biological properties of biodegradable WE43 alloy modified by Al ion implantation, Ceram. Int. 49 (2023) 5327–5334, https://doi.org/10.1016/j.ceramint.2022.10.056.

[23] D. Ma, K. Zhang, B. Dong, J. She, Y. Zhang, Study of hydroxyapatite-coated high-strength biodegradable magnesium-based alloy in repairing fracture damage in rats, In Vivo 37 (2023) 190–203, https://doi.org/10.21873/invivo.13068.

[24] J. Espiritu, M. Berangi, H. Cwieka, K. Iskhakova, A. Kuehne, D.C.F. Wieland, B. Zeller-Plumhoff, T. Niendorf, R. Willumeit-Roemer, J.M. Seitz, Radiofrequency induced heating of biodegradable orthopaedic screw implants during magnetic resonance imaging, Bioact. Mater. 25 (2023) 86–94, https://doi.org/10.1016/j.bioactmat.2023.01.017.

[25] M.K. Lei, P. Li, H.G. Yang, X.M. Zhu, Wear and corrosion resistance of Al ion implanted AZ31 magnesium alloy, Surf. Coat. Technol. 201 (2007) 5182–5185, https://doi.org/10.1016/j.surfcoat.2006.07.091.

[26] X. Liu, Z. Yue, T. Romeo, J. Weber, T. Scheuermann, S. Moulton, G. Wallace, Biofunctionalized anti-corrosive silane coatings for magnesium alloys, Acta Biomater. 9 (2013) 8671–8677, https://doi.org/10.1016/j.actbio.2012.12.025.

[27] H. Tang, Y. Gao, Preparation and characterization of hydroxyapatite containing coating on AZ31 magnesium alloy by micro-arc oxidation, J. Alloys Compd. 688 (2016) 699–708, https://doi.org/10.1016/j.jallcom.2016.07.079.

[28] S.K. Sharma, K.K. Saxena, K.B. Kumar, N. Kumar, The effect of reinforcements on the mechanical properties of AZ31 composites prepared by powder metallurgy: an overview, in: International Conference on Applied Research and Engineering (ICARAE), SOUTH AFRICA, Cape Town, 2021, pp. 2293–2299, https://doi.org/10.1016/j.matpr.2021.11.639.

[29] Y.B. Bozkurt, A. Celik, Tailoring biodegration rate of AZ31 magnesium alloy, Electrochim. Acta 435 (2022), https://doi.org/10.1016/j.electacta.2022.141403.

[30] S.A. Rahim, M.A. Joseph, T. Hanas, Tailoring biomineralization and biodegradation of Mg-Ca alloy by acetic acid pickling, Mater. Res. Express 7 (2020), https://doi.org/10.1016/j.electacta.2022.141403.

[31] N.M. Bexiga, M.M. Alves, M.G. Taryba, S.N. Pinto, M.F. Montemor, Early biomimetic degradation of Mg-2Ca alloy reveals the impact of β-phases at the interface of this biomaterial on a micro-scale level, Corros. Sci. 207 (2022), https://doi.org/10.1016/j.corsci.2022.110526.

[32] M.P. Sealy, Y.B. Guo, Surface integrity and process mechanics of laser shock peening of novel biodegradable magnesium-calcium (Mg-Ca) alloy, J. Mech. Behav. Biomed. Mater. 3 (2010) 488–496, https://doi.org/10.1016/j.jmbbm.2010.05.003.

[33] Z. Zhang, X. Sun, J. Yang, C. Wang, In vitro evaluation of freeze-drying chitosan-mineralized collagen/Mg-Ca alloy composites for osteogenesis, J. Biomater. Appl. 36 (2022) 1359–1377, https://doi.org/10.1177/08853282211049296.

[34] C. Wang, H. Fang, X. Qi, C. Hang, Y. Sun, Z. Peng, W. Wei, Y. Wang, Silk fibroin film-coated MgZnCa alloy with enhanced in vitro and in vivo performance prepared using surface activation, Acta Biomater. 91 (2019) 99–111, https://doi.org/10.1016/j.actbio.2019.04.048.

[35] J.-Y. Bae, E.-J. Gwak, G.-S. Hwang, H.W. Hwang, D.-J. Lee, J.-S. Lee, Y.-C. Joo, J.-Y. Sun, S.H. Jun, M.-R. Ok, J.-Y. Kim, S.-K. Kang, Biodegradable metallic glass for stretchable transient electronics, Adv. Sci. 8 (2021), https://doi.org/10.1002/advs.202004029.

[36] J.A.M. Carvalho, G. Domingues, M.T. Fernandes, N. Larcher, A.A. Ribeiro, J.A. Castro, Evaluation of MgZnCa alloys fabricated via powder metallurgy for manufacturing biodegradable surgical implants, Jom 73 (2021) 2403–2412, https://doi.org/10.1007/s11837-021-04739-2.

[37] V.K.N. Murali, M.S. Starvin, J.B. Raj, EXPLORING the corrosion inhibition of magnesium by coatings formulated with nano CeO and ZrO particles, Bull. Chem. Soc. Ethiop. 37 (2023) 1299–1306, https://doi.org/10.4314/bcse.v37i5.20.

[38] S. Amukarimi, I. Mobasherpour, B. Yarmand, P. Brouki-Milan, M. Mozafari, Synthesis, microstructure and biodegradation behavior of MgO-$TiO_2$-PCL nanocomposite coatings on the surface of magnesium-based biomaterials, Mater. Lett. 310 (2022), https://doi.org/10.1016/j.matlet.2021.131142.

[39] J. Manzur, M. Akhtar, A. Aizaz, K. Ahmad, M. Yasir, B.Z. Minhas, E. Avcu, M.A.U. Rehman, Electrophoretic deposition, microstructure, and selected properties of poly(lactic-co-glycolic) acid-based antibacterial coatings on Mg substrate, ACS Omega 8 (2023) 18074–18089, https://doi.org/10.1021/acsomega.3c01384.

[40] W. Wang, P. Wan, C. Liu, L. Tan, W. Li, L. Li, K. Yang, Degradation and biological properties of Ca-P contained micro-arc oxidation self-sealing coating on pure magnesium for bone fixation, Regener, Biomater 2 (2015) 107–118, https://doi.org/10.1093/rb/rbu014.

[41] A. Keyvani, N. Kamkar, R. Chaharmahali, M. Bahamirian, M. Kaseem, A. Fattah-alhosseini, Improving anti-corrosion properties AZ31 Mg alloy corrosion behavior in a simulated body fluid using plasma electrolytic oxidation coating containing hydroxyapatite nanoparticles, Inorg. Chem. Commun. 158 (2023), https://doi.org/10.1016/j.inoche.2023.111470.

[42] J.-n. Qin, J.-l. Wang, J. Pei, B.w. Xiong, Y.-p. Lei, J.-p. Li, A cage-structured protecting coating prepared on pure magnesium by hydrothermal treatment with enhanced corrosion properties, Mater. Today Commun. 25 (2020), https://doi.org/10.1016/j.mtcomm.2020.101645.

[43] L.-Y. Li, L.-Y. Cui, B. Liu, R.-C. Zeng, X.-B. Chen, S.-Q. Li, Z.-L. Wang, E.-H. Han, Corrosion resistance of glucose-induced hydrothermal calcium phosphate coating on pure magnesium, Appl. Surf. Sci. 465 (2019) 1066–1077, https://doi.org/10.1016/j.apsusc.2018.09.203.

[44] M. Tomozawa, S. Hiromoto, Growth mechanism of hydroxyapatite-coatings formed on pure magnesium and corrosion behavior of the coated magnesium, Appl. Surf. Sci. 257 (2011) 8253–8257, https://doi.org/10.1016/j.apsusc.2011.04.087.

[45] Front Matter, in: Magnesium – Alloys and Technology, 2003.

[46] R.L. Edgar, R. Schmid-Fetzer, J. Grbner, D. Kevorkov, F.G. Rammerstorfer, Magnesium Alloys and Their Applications, 2006.

[47] Abbott, B. Trevor, Magnesium: industrial and research developments over the last 15 years, Corrosion -Houston Tx- 71 (2015) 120–127, https://doi.org/10.5006/1474.

[48] M. Avedesian, H. Baker, ASM Specialty Handbook-Magnesium and Magnesium Alloys, 1999.

[49] H. Hyung-Seop, L. Sergio, J. Indong, E. James, K. Yu-Chan, S. Hyun-Kwang, W. Frank, M. Diego, G.J. Sion, Current status and outlook on the clinical translation of biodegradable metals, Mater. Today (2018), https://doi.org/10.1016/j.mattod.2018.05.018. S136970211830347X-.

[50] A. Fattah-Alhosseini, R. Chaharmahali, K. Babaei, M. Nouri, M.K. Keshavarz, M. Kaseem, A review of effective strides in amelioration of the biocompatibility of PEO coatings on Mg alloys, J. Magnesium Alloys 10 (2022) 2354–2383, https://doi.org/10.1016/j.jma.2022.09.002.

[51] K. Munir, J. Lin, C. Wen, P.F.A. Wright, Y. Li, Mechanical, corrosion, and biocompatibility properties of Mg-Zr-Sr-Sc alloys for biodegradable implant applications, Acta Biomater. 102 (2019), https://doi.org/10.1016/j.actbio.2019.12.001.

[52] S. Cifuentes, V.S. Miguel, W. Yu, A. García-Peas, Bioresorbable Metals for Cardiovascular and Fracture Repair Implants, Nanohybrids, 2021.

[53] D.M. Lamontanaro, Dental Restoration, Rt Image, 2006.

[54] S. Heise, Development of Advanced Chitosan-Based Biodegradable Coatings for Mg Alloys with Potential Applications in Orthopedic Implants, 2019.

[55] M. Esmaily, J.E. Svensson, S. Fajardo, N. Birbilis, G.S. Frankel, S. Virtanen, R. Arrabal, S. Thomas, L.G. Johansson, Fundamentals and advances in magnesium alloy corrosion, Prog. Mater. Sci. 89 (2017) 92–193, https://doi.org/10.1016/j.pmatsci.2017.04.011.

[56] E.C. Huse, A. New Ligature, Chic Med J Exam 37 (1878) 171–172.

[57] D.A. Vermilyea, C.F. Kirk, Studies of inhibition of magnesium corrosion, J. Electrochem. Soc. 116 (1969) 1375–1380, https://doi.org/10.1149/1.2411579.

[58] Y. Al-Abdullat, S. Tsutsumi, N. Nakajima, M. Ohta, H. Kuwahara, K. Ikeuchi, Surface modification of magnesium by $NaHCO_3$ and corrosion behavior in Hank's solution for new biomaterial applications, Mater. Trans. 42 (2001) 1777–1780, https://doi.org/10.2320/matertrans.42.1777.

[59] X. Lu, M. Mohedano, C. Blawert, E. Matykina, R. Arrabal, K.U. Kainer, M.L. Zheludkevich, Plasma electrolytic oxidation coatings with particle additions - a review, Surf. Coat. Technol. 307 (2016) 1165–1182, https://doi.org/10.1016/j.surfcoat.2016.08.055.

[60] T.S.N.S. Narayanan, I.S. Park, M.H. Lee, Strategies to improve the corrosion resistance of microarc oxidation (MAO) coated magnesium alloys for degradable implants: prospects and challenges, Prog. Mater. Sci. 60 (2014) 1–71, https://doi.org/10.1016/j.pmatsci.2013.08.002.

[61] A. Fattah-alhosseini, R. Chaharmahali, A. Rajabi, K. Babaei, M. Kaseem, Performance of PEO/polymer coatings on the biodegradability, antibacterial effect and biocompatibility of Mg-based materials, J. Funct. Biomater. 13 (2022), https://doi.org/10.3390/jfb13040267.

[62] T. Zehra, A. Fattah-alhosseini, M. Kaseem, Surface properties of plasma electrolytic oxidation coating modified by polymeric materials: a review, Prog. Org. Coat. 171 (2022), https://doi.org/10.1016/j.porgcoat.2022.107053.

[63] A. Fattah-Alhosseini, R. Chaharmahali, K. Babaei, M. Nouri, M.K. Keshavarz, M. Kaseem, A review of effective strides in amelioration of the biocompatibility of PEO coatings on Mg alloys, J. Magnesium Alloys 10 (2022) 2354–2383, https://doi.org/10.1016/j.jma.2022.09.002.

[64] S. Wu, Y.S. Jang, Y.K. Kim, S.Y. Kim, S.O. Ko, M.H. Lee, Surface modification of pure magnesium mesh for guided bone regeneration: in vivo evaluation of rat calvarial defect, Materials 12 (2019), https://doi.org/10.3390/ma12172684.

[65] A. Seyfoori, S. Mirdamadi, A. Khavandi, Z.S. Raufi, Biodegradation behavior of micro-arc oxidized AZ31 magnesium alloys formed in two different electrolytes, Appl. Surf. Sci. 261 (2012) 92–100, https://doi.org/10.1016/j.apsusc.2012.07.105.

[66] Y. Husak, J. Michalska, O. Oleshko, V. Korniienko, K. Grundsteins, B. Dryhval, S. Altundal, O. Mishchenko, R. Viter, M. Pogorielov, W. Simka, Bioactivity performance of pure Mg after plasma electrolytic oxidation in silicate-based solutions, Molecules 26 (2021), https://doi.org/10.3390/molecules26072094.

[67] W.H. Ma, Y.J. Liu, W. Wang, Y.Z. Zhang, Improved biological performance of magnesium by micro-arc oxidation, Braz. J. Med. Biol. Res. 48 (2015) 214–225, https://doi.org/10.1590/1414-431X20144171.

[68] Y. Han, Y. Yan, C. Lu, Y. Zhang, K. Xu, Bioactivity and osteoblast response of the micro-arc oxidized zirconia films, J. Biomed. Mater. Res. A. 88A (2009) 117–127, https://doi.org/10.1002/jbm.a.31859.

[69] M. Echeverry-Rendon, V. Duque, D. Quintero, S.M. Robledo, M.C. Harmsen, F. Echeverria, Improved corrosion resistance of commercially pure magnesium after its modification by plasma electrolytic oxidation with organic additives, J. Biomater. Appl. 33 (2018) 725–740, https://doi.org/10.1177/0885328218809911.

[70] W. Wang, P. Wan, C. Liu, L. Tan, W. Li, L. Li, K. Yang, Degradation and biological properties of Ca-P contained micro-arc oxidation self-sealing coating on pure magnesium for bone fixation, Regener, Biomater 2 (2014) 107–118, https://doi.org/10.1093/rb/rbu014.

[71] A. Alabbasi, A. Mehjabeen, M.B. Kannan, Q. Ye, C. Blawert, Biodegradable polymer for sealing porous PEO layer on pure magnesium: an in vitro degradation study, Appl. Surf. Sci. 301 (2014) 463–467, https://doi.org/10.1016/j.apsusc.2014.02.100.

[72] L. Mu, Z. Ma, J. Wang, S. Yuan, M. Li, Corrosion behavior and biological activity of micro arc oxidation coatings with berberine on a pure magnesium surface, Coatings 10 (2020), https://doi.org/10.3390/coatings10090837.

[73] M. Li, J. Liu, J. Li, Y. Li, S. Lu, Y. Yuan, The enhanced corrosion resistance of UMAO coatings on Mg by silane treatment, Prog. Nat. Sci.: Mater. Int. 24 (2014) 486–491, https://doi.org/10.1016/j.pnsc.2014.09.004.

[74] C. Blawert, W. Dietzel, E. Ghali, G. Song, Anodizing treatments for magnesium alloys and their effect on corrosion resistance in various environments, Adv. Eng. Mater. 8 (2006) 511–533, https://doi.org/10.1002/adem.200500257.

[75] G.L. Makar, J. Kruger, Corrosion of magnesium, Int. Mater. Rev. 38 (2013) 138–153, https://doi.org/10.1179/imr.1993.38.3.138.

[76] S. Hiromoto, T. Shishido, A. Yamamoto, N. Maruyama, H. Somekawa, T. Mukai, Precipitation control of calcium phosphate on pure magnesium by anodization, Corros. Sci. 50 (2008) 2906–2913, https://doi.org/10.1016/j.corsci.2008.08.013.

[77] H.K. Lim, S.H. Byun, J.M. Woo, S.M. Kim, S.M. Lee, B.J. Kim, H.E. Kim, J.W. Lee, S.M. Kim, J.H. Lee, Biocompatibility and biocorrosion of hydroxyapatite-coated magnesium plate: animal experiment, Materials 10 (2017), https://doi.org/10.3390/ma10101149.

[78] S. Ono, N. Masuko, Anodic films grown on magnesium and magnesium alloys in fluoride solutions, in: Magnesium Alloys 2003 Pt, vol. 2, 2003, https://doi.org/10.4028/www.scientific.net/MSF.419-422.897.

[79] S. Ono, H. Kijima, N. Masuko, Microstructure and voltage-current characteristics of anodic films formed on magnesium in electrolytes containing fluoride, Mater. Trans. 44 (2003) 539–545, https://doi.org/10.2320/matertrans.44.539.

[80] F. Peng, D. Wang, X. Ma, H. Zhu, Y. Qiao, X. Liu, "Petal effect"-inspired superhydrophobic and highly adhesive coating on magnesium with enhanced corrosion resistance and biocompatibility, Sci. China Mater. 61 (2017) 629–642, https://doi.org/10.1007/s40843-017-9087-2.

[81] Y. Liang, N. Hilal, P. Langston, V. Starov, Interaction forces between colloidal particles in liquid: theory and experiment, Adv. Colloid Interface Sci. 134–35 (2007) 151–166, https://doi.org/10.1016/j.cis.2007.04.003.

[82] F. Peng, H. Li, D. Wang, P. Tian, Y. Tian, G. Yuan, D. Xu, X. Liu, Enhanced corrosion resistance and biocompatibility of magnesium alloy by Mg-Al-layered double hydroxide, ACS Appl. Mater. Interfaces 8 (2016) 35033–35044, https://doi.org/10.1021/acsami.6b12974.

[83] Q. Wang, D. O'Hare, Recent advances in the synthesis and application of layered double hydroxide (LDH) nanosheets, Chem. Rev. 112 (2012) 4124–4155, https://doi.org/10.1021/cr200434v.

[84] C. Del Hoyo, Layered double hydroxides and human health: an overview, Appl. Clay Sci. 36 (2007) 103–121, https://doi.org/10.1016/j.clay.2006.06.010.

[85] K. Hosni, O. Abdelkarim, N. Frini-Srasra, E. Srasra, Synthesis, structure and photocatalytic activity of calcined Mg-Al-Ti-layered double hydroxides, Korean J. Chem. Eng. 32 (2015) 104–112, https://doi.org/10.1007/s11814-014-0199-8.

[86] F.-F. Chen, Y.-J. Zhu, Z.-C. Xiong, T.-W. Sun, Y.-Q. Shen, Highly flexible superhydrophobic and fire-resistant layered inorganic paper, ACS Appl. Mater. Interfaces 8 (2016) 34715–34724, https://doi.org/10.1021/acsami.6b12838.

[87] X. Hong, X. Gao, L. Jiang, Application of superhydrophobic surface with high adhesive force in no lost transport of superparamagnetic microdroplet, J. Am. Chem. Soc. 129 (2007) 1478, https://doi.org/10.1021/ja065537c.

[88] S.Y. Lee, S. Shrestha, B.K. Shrestha, C.H. Park, C.S. Kim, Covalent surface functionalization of bovine serum albumin to magnesium surface to provide robust corrosion inhibition and enhance in vitro osteo-inductivity, Polymers 12 (2020), https://doi.org/10.3390/polym12020439.

[89] B. Ratna Sunil, T.S. Sampath Kumar, U. Chakkingal, V. Nandakumar, M. Doble, Friction stir processing of magnesium-nanohydroxyapatite composites with controlled in vitro degradation behavior, Mater. Sci. Eng. C Mater. Biol. Appl. 39 (2014) 315–324, https://doi.org/10.1016/j.msec.2014.03.004.

[90] A.L. Rudd, C.B. Breslin, F. Mansfeld, The corrosion protection afforded by rare earth conversion coatings applied to magnesium, Corros. Sci. 42 (2000) 275–288, https://doi.org/10.1016/S0010-938X(99)00076-1.

[91] X. Liu, P.K. Chu, C. Ding, Surface nano-functionalization of biomaterials, Mat. Sci. Eng. R. 70 (2010) 275–302, https://doi.org/10.1016/j.mser.2010.06.013.

[92] R. Beutner, J. Michael, B. Schwenzer, D. Scharnweber, Biological nano-functionalization of titanium-based biomaterial surfaces: a flexible toolbox, J. R. Soc. Interface 7 (2010) S93–S105, https://doi.org/10.1098/rsif.2009.0418.focus.

[93] G. Calabrese, D. Franco, S. Petralia, F. Monforte, G.G. Condorelli, S. Squarzoni, F. Traina, S. Conoci, Dual-functional nano-functionalized titanium scaffolds to inhibit bacterial growth and enhance osteointegration, Nanomaterials 11 (2021), https://doi.org/10.3390/nano11102634.

[94] X. Ma, W. Huang, Z. Niu, W. Li, D. Mei, S. Zhu, S. Guan, A drug-loaded bio-functional anticorrosion coating on Mg alloy for orthopedic applications, Mater. Lett. 311 (2022) 131581, https://doi.org/10.1016/j.matlet.2021.131581.

[95] M.Z. Baghbaderani, S. Abazari, H.R. Bakhsheshi-Rad, A.F. Ismail, S. Sharif, A. Najafinezhad, S. Ramakrishna, M. Daroonparvar, F. Berto, Dual synergistic effects of MgO-go fillers on degradation behavior, biocompatibility and antibacterial activities of chitosan coated Mg alloy, Coatings 12 (2022), https://doi.org/10.3390/coatings12010063.

[96] N. Mehri Ghahfarokhi, B. Shayegh Broujeny, A. Hakimizad, A. Doostmohammadi, Plasma electrolytic oxidation (PEO) coating to enhance in vitro corrosion resistance of AZ91 magnesium alloy coated with polydimethylsiloxane (PDMS), Appl. Phys. A-Mater. 128 (2022), https://doi.org/10.1007/s00339-021-05239-5.

[97] Z. Song, Z. Xie, L. Ding, Y. Zhang, X. Hu, Preparation of corrosion-resistant MgAl-LDH/Ni composite coating on Mg alloy AZ31B, Colloid. Surface. A. 632 (2022), https://doi.org/10.1016/j.colsurfa.2021.127699.

[98] J. Dong, J. Zhong, R. Hou, X. Hu, Y. Chen, H. Weng, Z. Zhang, B. Liu, S. Yang, Z. Peng, Polymer bilayer-Micro arc oxidation surface coating on pure magnesium for bone implantation, J. Orthop. Transl. 40 (2023) 27–36, https://doi.org/10.1016/j.jot.2023.05.003.

[99] Z.-Z. Yin, W.-C. Qi, R.-C. Zeng, X.-B. Chen, C.-D. Gu, S.-K. Guan, Y.-F. Zheng, Advances in coatings on biodegradable magnesium alloys, J. Magnesium Alloys 8 (2020) 42–65, https://doi.org/10.1016/j.jma.2019.09.008.

[100] H. Hornberger, S. Virtanen, A.R. Boccaccini, Biomedical coatings on magnesium alloys - a review, Acta Biomater. 8 (2012) 2442–2455, https://doi.org/10.1016/J.ACTBIO.2012.04.012.

[101] M.D. Pereda, C. Alonso, M. Gamero, J.A. del Valle, M. Fernandez Lorenzo de Mele, Comparative study of fluoride conversion coatings formed on biodegradable powder metallurgy Mg: the effect of chlorides at physiological level, Mat. Sci. Eng. C-Mater. 31 (2011) 858–865, https://doi.org/10.1016/j.msec.2011.01.010.

[102] X.B. Chen, H.Y. Yang, T.B. Abbott, M.A. Easton, N. Birbilis, Corrosion protection of magnesium and its alloys by metal phosphate conversion coatings, Surf. Eng. 30 (2014) 871–879, https://doi.org/10.1179/1743294413Y.0000000235.

[103] S. Cheng, D. Zhang, M. Li, X. Liu, Y. Zhang, S. Qian, F. Peng, Osteogenesis, angiogenesis and immune response of Mg-Al layered double hydroxide coating on pure Mg, Bioact. Mater. 6 (2021) 91–105, https://doi.org/10.1016/j.bioactmat.2020.07.014.

[104] Z. Hu, X. Zhang, Z. Liu, K. Huo, P.K. Chu, J. Zhai, L. Jiang, Regulating water adhesion on superhydrophobic $TiO_2$ nanotube arrays, Adv. Funct. Mater. 24 (2014) 6381–6388, https://doi.org/10.1002/adfm.201401462.

[105] S. Hiromoto, M. Tomozawa, Corrosion behavior of magnesium with hydroxyapatite coatings formed by hydrothermal treatment, Mater. Trans. 51 (2010) 2080–2087, https://doi.org/10.2320/matertrans.M2010192.

[106] J. Li, W. Xu, X. Lin, F. Cao, K. Yang, A Ca-deficientca-deficient hydroxyapatite (CDHA)/$MgF_2$ bi-layer coating with unique nano-scale topography on biodegradable high-purity Mg, Colloid. Surface. B 190 (2020) 110911, https://doi.org/10.1016/j.colsurfb.2020.110911.

[107] M. Takaya, Anodizing of magnesium alloy in KOH-$Al(OH)_3$ solutions, J. Jpn. Inst. Light Metals 37 (1987) 581–586, https://doi.org/10.2464/jilm.37.581.

[108] K. Huber, Closure to "discussion of 'anodic formation of coatings on magnesium, zinc, and cadmium' [kurt huber (pp. 376–382)]", J. Electrochem. Soc. 101 (1954) 334, https://doi.org/10.1149/1.2781258.

[109] L. Hernández, J.E. González, V. Barranco, Y. Veranes-Pantoja, J.C. Galván, G.R. Gattorno, Biomimetic hydroxyapatite (HAp) coatings on pure Mg and their physiological corrosion behavior, Ceram. Int. 48 (2022) 1208–1222, https://doi.org/10.1016/j.ceramint.2021.09.206.

[110] M. Tomozawa, S. Hiromoto, Microstructure of hydroxyapatite- and octacalcium phosphate-coatings formed on magnesium by a hydrothermal treatment at various pH values, Acta Mater. 59 (2011) 355–363, https://doi.org/10.1016/j.actamat.2010.09.041.

[111] X. Cao, Q. Ren, Y. Yang, X. Hou, Y. Yan, J. Hu, H. Deng, D. Yu, W. Lan, F. Pan, A new environmentally-friendly route to in situ form a high-corrosion-resistant nesquehonite film on pure magnesium, RSC Adv. 10 (2020) 35480–35489, https://doi.org/10.1039/d0ra04423g.

[112] L. Qiao, Y. Wang, W. Wang, M. Mohedano, C. Gong, J. Gao, The preparation and corrosion performance of self-assembled monolayers of stearic acid and MgO layer on pure magnesium, Mater. Trans. 55 (2014) 1337–1343, https://doi.org/10.2320/matertrans.M2014117.

[113] S. Nesic, M. Nordsveen, R. Nyborg, A mechanistic model for carbon dioxide corrosion of mild steel in the presence of protective iron carbonate films–Part 2: a numerical experiment, corrosion, The Journal of Science and Engineering (2003) 59, https://doi.org/10.5006/1.3277579.

[114] Y.E. Yayoglu, R.G. Toomey, N.B. Crane, N.D. Gallant, Laser machined micropatterns as corrosion protection of both hydrophobic and hydrophilic magnesium, J. Mech. Behav. Biomed. Mater. 125 (2022) 104920, https://doi.org/10.1016/j.jmbbm.2021.104920.

[115] J.H. Jo, B.G. Kang, K.S. Shin, H.E. Kim, B.D. Hahn, D.S. Park, Y.H. Koh, Hydroxyapatite coating on magnesium with $MgF_2$ interlayer for enhanced corrosion resistance and biocompatibility, J. Mater. Sci-Mater. M. 22 (2011) 2437–2447, https://doi.org/10.1007/s10856-011-4431-3.

[116] X. Liu, P. Chu, C. Ding, Surface modification of titanium, titanium alloys, and related materials for biomedical applications, Mater. Sci. Eng. R. 47 (2004) 49–121, https://doi.org/10.1016/j.mser.2004.11.001.

[117] I. Dinaharan, S. Zhang, G. Chen, Q. Shi, Assessment of Ti-6Al-4V particles as a reinforcement for AZ31 magnesium alloy-based composites to boost ductility incorporated through friction stir processing, J. Magnesium Alloys 10 (2022) 979–992, https://doi.org/10.1016/j.jma.2020.09.026.

[118] E.B. Moustafa, A. Melaibari, G. Alsoruji, A.M. Khalil, A.O. Mosleh, Tribological and mechanical characteristics of AA5083 alloy reinforced by hybridising heavy ceramic particles $Ta_2C$ & VC with light GNP and $Al_2O_3$ nanoparticles, Ceram. Int. 48 (2022) 4710–4721, https://doi.org/10.1016/j.ceramint.2021.11.007.

[119] K. Qiao, T. Zhang, K. Wang, S. Yuan, L. Wang, S. Chen, Y. Wang, K. Xue, W. Wang, Effect of multi-pass friction stir processing on the microstructure evolution and corrosion behavior of $ZrO_2$/AZ31 magnesium matrix composite, J. Mater. Res. Technol. 18 (2022) 1166–1179, https://doi.org/10.1016/j.jmrt.2022.02.127.

[120] E.B. Moustafa, A.V. Mikhaylovskaya, M.A. Taha, A.O. Mosleh, Improvement of the microstructure and mechanical properties by hybridizing the surface of AA7075 by hexagonal boron nitride with carbide particles using the FSP process, J. Mater. Res. Technol. 17 (2022) 1986–1999, https://doi.org/10.1016/j.jmrt.2022.01.150.

[121] Y. Vengesa, A. Fattah-alhosseini, H. Elmkhah, O. Imantalab, Influence of post-deposition annealing temperature on morphological, mechanical and electrochemical properties of CrN/CrAlN multilayer coating deposited by cathodic arc evaporation- physical vapor deposition process, Surf. Coat. Technol. 432 (2022), https://doi.org/10.1016/j.surfcoat.2022.128090.

[122] Z. Shen, G. Liu, R. Zhang, J. Dai, L. He, R. Mu, Thermal property and failure behavior of LaSmZrO thermal barrier coatings by EB-PVD, iScience 25 (2022), https://doi.org/10.1016/j.isci.2022.104106.

[123] B. Yuan, Y. Wang, A.Y. Elnaggar, I.H. El Azab, M. Huang, M.H.H. Mahmoud, S.M. El-Bahy, M. Guo, Physical vapor deposition of graphitic carbon nitride (g-C3N4) films on biomass substrate: optoelectronic performance evaluation and life cycle assessment, Adv. Compos. Hybrid Mater. 5 (2022) 813–822, https://doi.org/10.1007/s42114-022-00505-3.

[124] W. Diyatmika, J.P. Chu, B.T. Kacha, C.-C. Yu, C.-M. Lee, Thin film metallic glasses in optoelectronic, magnetic, and electronic applications: a recent update, Curr. Opin. Solid State Mater. Sci. 19 (2015) 95–106, https://doi.org/10.1016/j.cossms.2015.01.001.

[125] A. Etiemble, C.D. Loughian, M. Apreutesei, C. Langlois, S. Cardinal, J.M. Pelletier, J.F. Pierson, P. Steyer, Innovative Zr-Cu-Ag thin film metallic glass deposed by magnetron PVD sputtering for antibacterial applications, J. Alloys Compd. 707 (2017) 155–161, https://doi.org/10.1016/j.jallcom.2016.12.259.

[126] S.T. Rajan, A. Arockiarajan, Thin film metallic glasses for bioimplants and surgical tools: a review, J. Alloys Compd. 876 (2021), https://doi.org/10.1016/j.jallcom.2021.159939.

[127] S.T. Rajan, M. Das, P.S. Kumar, A. Arockiarajan, B. Subramanian, Biological performance of metal metalloid (TiCuZrPd:B) TFMG fabricated by pulsed laser deposition, Colloid. Surface. B. 202 (2021), https://doi.org/10.1016/j.colsurfb.2021.111684.

[128] U. Jeong, J. Han, K.P. Marimuthu, Y. Lee, H. Lee, Evaluation of mechanical properties of Zr-Cu-Al-Ni TFMG using nanoindentation, J. Mater. Res. Technol. 12 (2021) 2368–2382, https://doi.org/10.1016/j.jmrt.2021.04.030.

[129] P.-H. Kuo, S.-Y. Tsai, J.-G. Duh, Bio-compatible Zirconium-based thin film metallic glasses with nitrogen reinforced by micro-alloying technique, Mater. Chem. Phys. 272 (2021), https://doi.org/10.1016/j.matchemphys.2021.124965.

[130] R.S. Mishra, Z.Y. Ma, Friction stir welding and processing VIII, Materials ence & Engineering R 50 (2005) 1–78, https://doi.org/10.1016/j.mser.2005.07.001.

[131] R.S. Mishra, M.W. Mahoney, S.X. McFaden, N.A. Mara, A.K. Mukherjee, High strain rate superplasticity in a friction stir processed 7075 Al alloy, Scr. Mater. 42 (1999) 163–168, https://doi.org/10.1016/S1359-6462(99)00329-2.

[132] Qing-Hua Tang, Xiang-Shui Miao, Ge Wu, Chang Liu, Jian Lu, Novel multilayer structure design of metallic glass film deposited Mg alloy with superior mechanical properties and corrosion resistance, Intermetallics (2015), https://doi.org/10.1016/j.intermet.2015.02.019.

[133] T. Balusamy, T. Narayanan, K. Ravichandran, L.S. Park, H.L. Min, Influence of surface mechanical attrition treatment (SMAT) on the corrosion behaviour of AISI 304 stainless steel, Corros. Sci. 74 (2013) 332–344, https://doi.org/10.1016/j.corsci.2013.04.056.

[134] N.R. Tao, Z.B. Wang, W.P. Tong, M.L. Sui, J. Lu, K. Lu, An investigation of surface nanocrystallization mechanism in Fe induced by surface mechanical attrition treatment, Acta Mater. (2002) 50, https://doi.org/10.1016/S1359-6454(02)00310-5.

[135] S. Kumar, K. Chattopadhyay, G.S. Mahobia, V. Singh, Hot corrosion behaviour of Ti–6Al–4V modified by ultrasonic shot peening, Mater. Des. 110 (2016) 196–206, https://doi.org/10.1016/j.matdes.2016.07.133.

[136] X. Wu, N. Tao, Y. Hong, B. Xu, J. Lu, K. Lu, Microstructure and evolution of mechanically-induced ultrafine grain in surface layer of AL-alloy subjected to USSP, Acta Mater. 50 (2002) 2075–2084, https://doi.org/10.1016/S1359-6454(02)00051-4.

[137] R. Zhang, X. Zhou, H. Gao, S. Mankoci, Y. Liu, X. Sang, H. Qin, X. Hou, Z. Ren, G.L. Doll, The effects of laser shock peening on the mechanical properties and biomedical behavior of AZ31B magnesium alloy, Surf. Coat. Technol. 339 (2018) 48–56, https://doi.org/10.1016/j.surfcoat.2018.02.009.

[138] I. Altenberger, R.K. Nalla, Y. Sano, L. Wagner, R.O. Ritchie, On the effect of deep-rolling and laser-peening on the stress-controlled low- and high-cycle fatigue behavior of Ti–6Al–4V at elevated temperatures up to 550 °C, Int. J. Fatigue. 44 (2012) 292–302, https://doi.org/10.1016/j.ijfatigue.2012.03.008.

[139] H. Ye, X. Sun, Y. Liu, X.-x. Rao, Q. Gu, Effect of ultrasonic surface rolling process on mechanical properties and corrosion resistance of AZ31B Mg alloy, Surf. Coat. Technol. 372 (2019) 288–298, https://doi.org/10.1016/j.surfcoat.2019.05.035.

[140] Y. Liu, X. Zhao, D. Wang, Determination of the plastic properties of materials treated by ultrasonic surface rolling process through instrumented indentation, Mat. Sci. Eng. A-Struct. 600 (2014) 21–31, https://doi.org/10.1016/j.msea.2014.01.096.

[141] E. Ma, J. Xu, BIODEGRADABLE ALLOYS the glass window of opportunities, Nat. Mater. 8 (2009) 855–857, https://doi.org/10.1016/j.jde.2003.09.009.

[142] S. Gonzalez, E. Pellicer, J. Fornell, A. Blanquer, L. Barrios, E. Ibanez, P. Solsona, S. Surinach, M.D. Baro, C. Nogues, J. Sort, Improved mechanical performance and delayed corrosion phenomena in biodegradable Mg-Zn-Ca alloys through Pd-alloying, J. Mech. Behav. Biomed. Mater. 6 (2012) 53–62, https://doi.org/10.1016/j.jmbbm.2011.09.014.

[143] S.T. Rajan, A. Bendavid, B. Subramanian, Cytocompatibility assessment of Ti-Nb-Zr-Si thin film metallic glasses with enhanced osteoblast differentiation for biomedical applications, Colloids Surf., B 173 (2019) 109–120, https://doi.org/10.1016/j.colsurfb.2018.09.041.

[144] S.T. Rajan, A.K.N. Kumar, B. Subramanian, Nanocrystallization in magnetron sputtered Zr-Cu-Al-Ag thin film metallic glasses, CrystEngComm 16 (2014) 2835–2844, https://doi.org/10.1039/c3ce42294a.

[145] X.H. Lin, W.L. Johnson, Formation of Ti–Zr–Cu–Ni bulk metallic glasses, J. Appl. Phys. 78 (1995) 6514–6519, https://doi.org/10.1063/1.360537.

[146] C.H. Huang, J.C. Huang, J.B. Li, J.S.C. Jang, Simulated body fluid electrochemical response of Zr-based metallic glasses with different degrees of crystallization, Mat. Sci. Eng. C-Mater. 33 (2013) 4183–4187, https://doi.org/10.1016/j.msec.2013.06.007.

[147] X.H. Yan, J.S. Li, W.R. Zhang, Y. Zhang, A brief review of high-entropy films, Mater. Chem. Phys. 210 (2018) 12–19, https://doi.org/10.1016/j.matchemphys.2017.07.078.

[148] W.J. Zhang, Y. Li, S.L. Zhu, F.H. Wang, Influence of argon flow rate on $TiO_2$ photocatalyst film deposited by dc reactive magnetron sputtering, Surf. Coat. Technol. 182 (2004), https://doi.org/10.1016/j.surfcoat.2003.08.050.

[149] X. Feng, G. Tang, M. Sun, X. Ma, K. Yukimura, Structure and properties of multi-targets magnetron sputtered ZrNbTaTiW multi-elements alloy thin films, Surf. Coat. Technol. 228 (2013) S424–S427, https://doi.org/10.1016/j.surfcoat.2012.05.038.

[150] M. Mateev, T. Lautenschläger, D. Spemann, A. Finzel, J.W. Gerlach, F. Frost, C. Bundesmann, Systematic investigation of the reactive ion beam sputter deposition process of $SiO_2$, Eur. Phys. J. B 91 (2018), https://doi.org/10.1140/EPJB/E2018-80453-X.

[151] R. Feder, F. Frost, H. Neumann, C. Bundesmann, B. Rauschenbach, Systematic investigations of low energy Ar ion beam sputtering of Si and Ag, Nucl. Instrum. Methods Phys. Res. 317 (2013) 137–142, https://doi.org/10.1016/j.nimb.2013.01.056.

[152] C. Bundesmann, T. Lautenschl?Ger, D. Spemann, A. Finzel, E. Thelander, M. Mensing, F. Frost, Systematic investigation of the properties of $TiO_2$ films grown by reactive ion beam sputter deposition, Appl. Surf. Sci. S0169433216316981 (2017), https://doi.org/10.1016/j.apsusc.2016.08.056.

[153] M.Z. A, F.S. A, B.D. B, H.N. B, Optimisation and characterisation of a TCP type RF broad beam ion source, Surf. Coat. Technol. s 142–144 (2001) 39–48, https://doi.org/10.1016/j.apsusc.2016.08.056.

[154] S.S. Mao, High throughput growth and characterization of thin film materials, J. Cryst. Growth 379 (2013) 123–130, https://doi.org/10.1016/j.jcrysgro.2012.10.051.

[155] P. Schenck, K, J. Klamo, L, N. Bassim, D. Burke, Combinatorial study of the crystallinity boundary in the $HfO_2$–$TiO_2$–$Y_2O_3$ system using pulsed laser deposition library thin films, Thin Solid Films (2008), https://doi.org/10.1016/j.tsf.2008.08.001.

[156] S.S. Mao, X. Zhang, High-Throughput multi-plume pulsed-laser deposition for materials exploration and optimization, Engineering 1 (2015) 367–371, https://doi.org/10.15302/J-ENG-2015065.

[157] X. The, Bakerian Lecture. —experimental relations of gold (and other metals) to light, Philos. Trans. R. Soc. London, A 147 (1997) 145–181, https://doi.org/10.1098/rstl.1857.0011.

[158] R.J. Martín-Palma, A. Lakhtakia, Vapor-deposition techniques, in: Engineered Biomimicry, 2013, pp. 383–398, https://doi.org/10.1016/B978-0-12-415995-2.00015-5.

[159] K.A. Kravanja, M. Finšgar, A review of techniques for the application of bioactive coatings on metal-based implants to achieve controlled release of active ingredients, Mater. Des. 217 (2022), https://doi.org/10.1016/j.matdes.2022.110653.

[160] F.C. Li, T. Liu, J.Y. Zhang, S. Shuang, Q. Wang, A.D. Wang, J.G. Wang, Y. Yang, Amorphous–nanocrystalline alloys: fabrication, properties, and applications, Mater. Today Adv. 4 (2019), https://doi.org/10.1016/j.mtadv.2019.100027.

[161] P. Zhang, J.Y. Zhang, J. Li, G. Liu, K. Wu, Y.Q. Wang, J. Sun, Microstructural evolution, mechanical properties and deformation mechanisms of nanocrystalline Cu thin films alloyed with Zr, Acta Mater. 76 (2014) 221–237, https://doi.org/10.1016/j.actamat.2014.04.041.

[162] B.R. Braeckman, D. Depla, Structure formation and properties of sputter deposited $Nb_x$-CoCrCuFeNi high entropy alloy thin films, J. Alloys Compd. 646 (2015) 810–815, https://doi.org/10.1016/j.jallcom.2015.06.097.

[163] Z.-C. Chang, S.-C. Liang, S. Han, Y.-K. Chen, F.-S. Shieu, Characteristics of TiVCrAlZr multi-element nitride films prepared by reactive sputtering, Nucl.Instrum. Meth. B 268 (2010) 2504–2509, https://doi.org/10.1016/j.nimb.2010.05.039.

[164] Q. Cao, L. Lv, X. Wang, J. Jiang, Magnetron sputtering metal glass film preparation and the "specimen size Effect"of the mechanical property, Acta Metall. Sin. 57 (2021) 473–490, https://doi.org/10.11900/0412.1961.2020.00430.

[165] S. Korkmaz, I.A. Kariper, Glass formation, production and superior properties of Zr-based thin film metallic glasses (TFMGs): a status review, J. Non-Cryst. Solids 527 (2020), https://doi.org/10.1016/j.jnoncrysol.2019.119753.

[166] P. Yiu, N. Bonninghoff, J.P. Chu, Evaluation of Cr-based thin film metallic glass as a potential replacement of PVD chromium coating on plastic mold surface, Surf. Coat. Technol. 442 (2022), https://doi.org/10.1016/j.surfcoat.2022.128274.

[167] J.T. Gudmundsson, Physics and technology of magnetron sputtering discharges, Plasma Sources Sci. Technol. 29 (2020), https://doi.org/10.1088/1361-6595/abb7bd.

[168] J.C. Sagás, D.A. Duarte, S.F. Fissmer, Effect of oxygen concentration and system geometry on the current–voltage relations during reactive sputter deposition of titanium dioxide thin films, Vacuum 85 (2011) 1042–1046, https://doi.org/10.1016/j.vacuum.2011.03.015.

[169] J.Y. Bae, E.J. Gwak, G.S. Hwang, H.W. Hwang, D.J. Lee, J.S. Lee, Y.C. Joo, J.Y. Sun, S.H. Jun, M.R. Ok, J.Y. Kim, S.K. Kang, Biodegradable metallic glass for stretchable transient electronics, Adv. Sci. 8 (2021) 2004029, https://doi.org/10.1002/advs.202004029.

[170] J. Li, F.S. Gittleson, Y. Liu, J. Liu, A.M. Loye, L. McMillon-Brown, T.R. Kyriakides, J. Schroers, A.D. Taylor, Exploring a wider range of Mg-Ca-Zn metallic glass as biocompatible alloys using combinatorial sputtering, Chem. Commun. (Camb) 53 (2017) 8288–8291, https://doi.org/10.1039/c7cc02733h.

[171] G. Wu, Y. Liu, C. Liu, Q.-H. Tang, X.-S. Miao, J. Lu, Novel multilayer structure design of metallic glass film deposited Mg alloy with superior mechanical properties and corrosion resistance, Intermetallics 62 (2015) 22–26, https://doi.org/10.1016/j.intermet.2015.02.019.

[172] J. Liu, Y. Fu, Y. Tang, X.D. Wang, Q.P. Cao, D.X. Zhang, J.Z. Jiang, Thickness dependent structural evolution in Mg-Zn-Ca thin film metallic glasses, J. Alloys Compd. 742 (2018) 524–535, https://doi.org/10.1016/j.jallcom.2018.01.312.

[173] A. Datye, S. Alexander Kube, D. Verma, J. Schroers, U.D. Schwarz, Accelerated discovery and mechanical property characterization of bioresorbable amorphous alloys in the Mg-Zn-Ca and the Fe-Mg-Zn systems using high-throughput methods, J. Mater. Chem. B 7 (2019) 5392–5400, https://doi.org/10.1039/c9tb01302d.

[174] T.O. Olugbade, T.E. Abioye, P.K. Farayibi, N.G. Olaiya, B.O. Omiyale, T.I. Ogedengbe, Electrochemical properties of MgZnCa-based thin film metallic glasses fabricated by magnetron sputtering deposition coated on a stainless steel substrate, Anal. Lett. 54 (2020) 1588–1602, https://doi.org/10.1080/00032719.2020.1815757.

[175] S. Balasubramanian, Magnetron sputtered magnesium-based thin film metallic glasses for bioimplants, Biointerphases 16 (2021) 011005, https://doi.org/10.1116/6.0000535.
[176] K. Schlüter, C. Zamponi, N. Hort, K.U. Kainer, E. Quandt, Polycrystalline and amorphous MgZnCa thin films, Corros. Sci. 63 (2012) 234–238, https://doi.org/10.1016/j.corsci.2012.06.005.
[177] A. K.S, A. Rajeshwari, S. Kundu, S. B, Magnesium glassy alloy laminated nanofibrous polymer as biodegradable scaffolds, J. Non-Cryst. Solids 502 (2018) 210–217, https://doi.org/10.1016/j.jnoncrysol.2018.09.011.
[178] Y. Fu, Q.P. Cao, S.Y. Liu, C. Wang, X.D. Wang, D.X. Zhang, S.X. Qu, H.J. Fecht, J.Z. Jiang, Anomalous deformation mode transition in amorphous Mg-Zn-Ca thin films, Scr. Mater. 149 (2018) 139–143, https://doi.org/10.1016/j.scriptamat.2018.02.026.
[179] Swann, Magnetron sputtering, Phys. Technol. 19 (1988) 67, https://doi.org/10.1088/0305-4624/19/2/304.
[180] P.J. Kelly, R.D. Arnell, Magnetron sputtering: a review of recent developments and applications, Vacuum 56 (2000) 159–172, https://doi.org/10.1016/S0042-207X(99)00189-X.
[181] H. Ye, X. Sun, Y. Liu, X.X. Rao, Q. Gu, Effect of ultrasonic surface rolling process on mechanical properties and corrosion resistance of AZ31B Mg alloy, Surf. Coat. Technol. 372 (2019) 288–298, https://doi.org/10.1016/j.surfcoat.2019.05.035.
[182] R. Behrisch, W. Eckstein, Sputtering by Particle Bombardment/Experiments and Computer Calculations from Threshold to MeV Energies, Springer, 2007, https://doi.org/10.1007/978-3-540-44502-9.
[183] T. Serikawa, M. Henmi, T. Yamaguchi, H. Oginuma, K. Kondoh, Depositions and microstructures of Mg–Si thin film by ion beam sputtering, Surf. Coat. Technol. 200 (2006) 4233–4239, https://doi.org/10.1016/j.surfcoat.2005.01.047.
[184] J. Chen, H.B. Yang, Y.Y. Xia, N. Kuriyama, Q. Xu, T. Sakai, Hydriding and dehydriding properties of amorphous MagnesiumNickel films prepared by a sputtering method, Chem. Mater. 14 (2002) 2834, https://doi.org/10.1021/cm025502l, 2834.
[185] Y. Bohne, D.M. Seeger, C. Blawert, W. Dietzel, S. Mändl, B. Rauschenbach, Influence of ion energy on properties of Mg alloy thin films formed by ion beam sputter deposition, Surf. Coat. Technol. 200 (2006) 6527–6532, https://doi.org/10.1016/j.surfcoat.2005.11.088.
[186] M. Jelínek, V. Trtík, L. Jastrabík, Pulsed Laser Deposition of Thin Films, 1997, https://doi.org/10.1007/978-94-011-5732-2_16. Springer Netherlands.
[187] C. Combes, C. Rey, Amorphous calcium phosphates: synthesis, properties and uses in biomaterials, Acta Biomater. 6 (2010) 3362–3378, https://doi.org/10.1016/j.actbio.2010.02.017.
[188] P. Baeri, L. Torrisi, N. Marino, G. Foti, Ablation of hydroxyapatite by pulsed laser irradiation, Appl. Surf. Sci. 54 (1992) 210–214, https://doi.org/10.1016/0169-4332(92)90046-Z.
[189] H. Zeng, W.R. Lacefield, XPS, EDX and FTIR analysis of pulsed laser deposited calcium phosphate bioceramic coatings: the effects of various process parameters, Biomaterials 21 (2000) 23–30, https://doi.org/10.1016/S0142-9612(99)00128-3.
[190] C.M. Cotell, D.B. Chrisey, K.S. Grabowski, J.A. Sprague, C.R. Gossett, Pulsed laser deposition of hydroxylapatite thin films on Ti-6Al-4V, J. Appl. Biomater. 3 (2010) 87–93, https://doi.org/10.1002/jab.770030204.
[191] M. Störmer, C. Blawert, H. Hagen, V. Heitmann, W. Dietzel, Structure and corrosion of magnetron sputtered pure Mg films on silicon substrates, Plasma Processes Polym. 4 (2007) S557–S561, https://doi.org/10.1002/ppap.200731405.
[192] C. Blawert, V. Heitmann, N. Scharnagl, M. Strmer, J. Lutz, A. Prager-Duschke, D. Manova, S. Mndl, Different Underlying Corrosion Mechanism for Mg Bulk Alloys and Mg Thin Films, WILEY-VCH Verlag, 2009, https://doi.org/10.1002/ppap.200932405.
[193] Grigucevičienė Asta, Leinartas Konstantinas, Jušk ėnas Remigijus, Eimutis, Structure and initial corrosion resistance of sputter deposited nanocrystalline Mg–Al–Zr alloys, Mater. Sci. Eng. (2005), https://doi.org/10.1016/j.msea.2004.11.047.
[194] Y. Bohne, D.M. Seeger, C. Blawert, W. Dietzel, B. Rauschenbach, Influence of ion energy on properties of Mg alloy thin films formed by ion beam sputter deposition, Surf. Coat. Technol. 200 (2006) 6527–6532, https://doi.org/10.1016/j.surfcoat.2005.11.088.
[195] G. Garcés, S. Landais, P. Adeva, Effect of the substrate temperature on the microstructure and texture of Mg90Zr10 (at.%) films deposited by sputtering, J. Alloys Compd. 425 (2006) 148–152, https://doi.org/10.1016/j.jallcom.2006.01.015.
[196] Y. Bohne, D. Manova, C. Blawert, M. Störmer, W. Dietzel, S. Mändl, Deposition and properties of novel microcrystalline Mg alloy coatings, Surf. Eng. 23 (2007) 339–343, https://doi.org/10.1179/174329407X238884.
[197] F. Witte, V. Kaese, H. Haferkamp, E. Switzer, L.A. Meyer, C.J. Wirth, H. Windhagen, In vivo corrosion of four magnesium alloys and the associated bone response, Biomaterials (2005) 26, https://doi.org/10.1016/j.biomaterials.2004.09.049.
[198] V.D. Okunev, Z.A. Samoilenko, Amorphous state and pulsed laser deposition of YBa2Cu3O7δ thin films, J. Appl. Phys. 85 (1999) 7282–7290, https://doi.org/10.1016/10.1063/1.370545.
[199] S. Proyer, E. Stangl, M. Borz, D. Bäuerle, Particulates on pulsed-laser deposited Y•Ba•Cu•O films, Appl. Surf. Sci. s 96–98 (1996) 668–671, https://doi.org/10.1016/0921-4534(95)00678-8.
[200] S.J. Chung, A. Roy, D. Hong, J.P. Leonard, P.N. Kumta, Microstructure of Mg–Zn–Ca thin film derived by pulsed laser deposition, Mater. Sci. Eng., B 176 (2011) 1690–1694, https://doi.org/10.1016/j.mseb.2011.08.006.
[201] S. Ningshen, U. Kamachi Mudali, R. Krishnan, B. Raj, Corrosion behavior of Zr-based metallic glass coating on type 304L stainless steel by pulsed laser deposition method, Surf. Coat. Technol. 205 (2011) 3961–3966, https://doi.org/10.1016/j.surfcoat.2011.02.039.
[202] Y. Tian, M. Womack, P. Molian, C.C.H. Lo, J.W. Anderegg, A.M. Russell, Microstructure and nanomechanical properties of Al–Mg–B–Ti films synthesized by pulsed laser deposition, Thin Solid Films 418 (2002) 129–135, https://doi.org/10.1016/S0040-6090(02)00766-6.
[203] W. Gao, Z. Li, N. Sammes, An Introduction to Electronic Materials for Engineers, an Introduction to Electronic Materials for Engineers, second ed., 2011.
[204] B. Clarke, Normal bone anatomy and physiology, Clin. J. Am. Soc. Nephrol. 3 (Suppl 3) (2008) S131, https://doi.org/10.2215/CJN.04151206.
[205] M. C, E. Schoenfeld, P, P. Lautenschlager, R. Meyer Jr., Mechanical properties of human cancellous bone in the femoral head, Med. Biol. Eng. (1974), https://doi.org/10.1007/BF02477797.
[206] W.R. Walsh, M.H. Pelletier, N. Bertollo, V. Lovric, T. Wang, P. Morberg, W.C.H. Parr, D. Bergadano, Bone ongrowth and mechanical fixation of implants in cortical and cancellous bone, J. Orthop. Surg. Res. 15 (2020), https://doi.org/10.1186/s13018-020-01696-5.
[207] B.Q. Le, V. Nurcombe, M.K. Cool, C.A.V. Blitterswijk, J.D. Boer, V.L.S. Lapointe, The Components of Bone and what They Can Teach Us about Regeneration, MDPI, 2017, https://doi.org/10.3390/ma11010014.
[208] R.F. Heary, P. Naresh, S. Sujitha, A. Nitin, Elastic modulus in the selection of interbody implants, J. of Spine Surgery 3 (2017) 163, https://doi.org/10.21037/jss.2017.05.01.
[209] R.B. Ashman, J.Y. Rho, Elastic modulus of trabecular bone material, J. Biomech. 21 (1988) 177–181, https://doi.org/10.1016/0021-9290(88)90167-4.
[210] M. He, L. Chen, M. Yin, S. Xu, Z. Liang, Review on magnesium and magnesium-based alloys as biomaterials for bone immobilization, J. Mater. Res. Technol. 23 (2023) 4396–4419, https://doi.org/10.1016/j.jmrt.2023.02.037.
[211] A. Bonicelli, E.F. Kranioti, B. Xhemali, E. Arnold, P. Zioupos, Assessing bone maturity: compositional and mechanical properties of rib cortical bone at different ages, Bone 155 (2022) 116265, https://doi.org/10.1016/j.bone.2021.116265.
[212] Y. Zhang, J. Xu, Y.C. Ruan, M.K. Yu, M. O'Laughlin, H. Wise, D. Chen, L. Tian, D. Shi, J. Wang, S. Chen, J.Q. Feng, D.H.K. Chow, X. Xie, L. Zheng, L. Huang, S. Huang, K. Leung, N. Lu, L. Zhao, H. Li, D. Zhao, X. Guo, K. Chan, F. Witte, H.C. Chan, Y. Zheng, L. Qin, Implant-derived magnesium induces local neuronal production of CGRP to improve bone-fracture healing in rats, Nat. Med. 22 (2016) 1160–1169, https://doi.org/10.1038/nm.4162.
[213] Y. Dai, Y. Tang, X. Xu, Z. Luo, Y. Zhang, Z. Li, Z. Lin, S. Zhao, M. Zeng, B. Sun, Evaluation of the mechanisms and effects of Mg-Ag-Y alloy on the tumor growth and metastasis of the MG63 osteosarcoma cell line, J. Biomed. Mater. Res. B. 107 (2019) 2537–2548, https://doi.org/10.1002/jbm.b.34344.
[214] J. Fei, X. Wen, X. Lin, Saijilafu, W. Wang, O. Ren, X. Chen, L. Tan, K. Yang, H. Yang, Biocompatibility and neurotoxicity of magnesium alloys potentially used for neural repairs, Mat. Sci. Eng. C 78 (2017) 1155, https://doi.org/10.1016/j.msec.2017.04.106.
[215] D. Li, D. Zhang, Q. Yuan, L. Liu, H. Li, L. Xiong, X. Guo, Y. Yan, K. Yu, Y. Dai, In vitro and in vivo assessment of the effect of biodegradable magnesium alloys on osteogenesis, Acta Biomater. 141 (2022) 454–465, https://doi.org/10.1016/j.actbio.2021.12.032.

[216] G.U. A, A.T. A, A.C. A, S.B. B, Magnesium based implants for functional bone tissue regeneration – a review, J. Magnesium Alloys 10 (2022) 356–386, https://doi.org/10.1016/j.actbio.2021.12.032.
[217] P. Zhi, L. Liu, J. Chang, C. Liu, Q. Zhang, J. Zhou, Z. Liu, Y. Fan, Advances in the study of magnesium alloys and their use in bone implant material, Metals 12 (2022), https://doi.org/10.3390/met12091500.
[218] I. Antoniac, M. Miculescu, V.M. Pltnea, A. Stere, P.H. Quan, G. Pltnea, A. Robu, K. Earar, Magnesium-based alloys used in orthopedic surgery, Materials 15 (2022), https://doi.org/10.3390/ma15031148.
[219] A.A. Al-Tamimi, P.R.A. Fernandes, C. Peach, G. Cooper, P.J. Bartolo, Metallic bone fixation implants: a novel design approach for reducing the stress shielding phenomenon, Virtual Phys. Prototy. 12 (2017), https://doi.org/10.1080/17452759.2017.1307769.
[220] V. Bazhenov, A. Koltygin, A. Komissarov, A. Li, Y. Estrin, Gallium-containing magnesium alloy for potential use as temporary implants in osteosynthesis, J. Magnesium Alloys 8 (2020), https://doi.org/10.1016/j.jma.2020.02.009.
[221] C.S. Bala, Magnesium based implants for functional bone tissue regeneration–A review, J. Magnesium Alloys 10 (2022) 384–419, https://doi.org/10.1016/j.jma.2021.08.017.
[222] X. Lin, S. Yang, K. Lai, H. Yang, T.J. Webster, L. Yang, Orthopedic implant biomaterials with both osteogenic and anti-infection capacities and associated in vivo evaluation methods, Nanomedicine (2017) S1549963416301113, https://doi.org/10.1016/j.nano.2016.08.003.
[223] M. Ren, S. Cai, T. Liu, et al., Calcium phosphate glass/$MgF_2$ double layered composite coating for improving the corrosion resistance of magnesium alloy, J. Alloys Compd. 591 (2014) 34–40, https://doi.org/10.1016/j.jallcom.2013.12.215.
[224] Calin Mariana, Gebert Annett, Cosmina Andreea, PetreFlaviu Ghinea, Designing biocompatible Ti-based metallic glasses for implant applications, Mat. Sci. Eng. C (2013), https://doi.org/10.1016/j.msec.2012.11.015.
[225] J.E. Park, J.E. Park, Y.S. Jang, Y.S. Jang, J.B. Choi, J.B. Choi, T.S. Bae, T.S. Bae, I.S. Park, I.S. Park, Evaluation of corrosion behavior and in vitro of strontium-doped calcium phosphate coating on magnesium, Materials 14 (2021) 6625, https://doi.org/10.3390/ma14216625.
[226] A. Bakkar, V. Neubert, Improving corrosion resistance of magnesium-based alloys by surface modification with hydrogen by electrochemical ion reduction (EIR) and by plasma immersion ion implantation (PIII), Corros. Sci. 47 (2005) 1211–1225, https://doi.org/10.1016/j.corsci.2004.06.027.
[227] Y. Zhu, K. Yang, R. Cheng, Y. Xiang, T. Yuan, B. Sarmento, Y. Cheng, W. Cui, The current status of biodegradable stent to treat benign luminal disease, Mater. Today (2017) S1369702117301177, https://doi.org/10.1016/j.mattod.2017.05.002.
[228] P. Chakraborty Banerjee, S. Al-Saadi, L. Choudhary, S. Harandi, R. Singh, Magnesium implants: prospects and challenges, Materials 12 (2019), https://doi.org/10.3390/ma12010136.
[229] L. Li, M. Zhang, Y. Li, J. Zhao, L. Qin, Y. Lai, Corrosion and biocompatibility improvement of magnesium-based alloys as bone implant materials: a review, Regener, Biomater 4 (2017) 9, https://doi.org/10.1093/rb/rbx004.
[230] S.B. Kim, J.H. Jo, S.M. Lee, H.E. Kim, K.H. Shin, Y.H. Koh, Use of a poly(ether imide) coating to improve corrosion resistance and biocompatibility of magnesium (Mg) implant for orthopedic applications, J. Biomed. Mater. Res. B. (2013), https://doi.org/10.1002/jbm.a.34474.
[231] L.-Y. Li, L.-Y. Cui, R.-C. Zeng, S.-Q. Li, X.-B. Chen, Y. Zheng, M.B. Kannan, Advances in functionalized polymer coatings on biodegradable magnesium alloys - a review, Acta Biomater. 79 (2018) 23–36, https://doi.org/10.1016/j.actbio.2018.08.030.
[232] D. Zhang, F. Peng, X. Liu, Protection of magnesium alloys: from physical barrier coating to smart self-healing coating, J. Alloys Compd. 853 (2021), https://doi.org/10.1016/j.jallcom.2020.157010.
[233] Y. Zhu, W. Liu, T. Ngai, Polymer coatings on magnesium-based implants for orthopedic applications, J. Polym. Sci. 60 (2022) 32–51, https://doi.org/10.1002/pol.20210578.
[234] C. Pan, X. Liu, Q. Hong, J. Chen, Y. Cheng, Q. Zhang, L. Meng, J. Dai, Z. Yang, L. Wang, Recent advances in surface endothelialization of the magnesium alloy stent materials, J. Magnesium Alloys 11 (2023) 48–77, https://doi.org/10.1016/j.jma.2022.12.017.
[235] S. Omanovic, S.G. Roscoe, Electrochemical studies of the adsorption behavior of bovine serum albumin on stainless steel, Langmuir 15 (1999) 8315–8321, https://doi.org/10.1021/la990474f.
[236] G.B. Hamu, D. Eliezer, L. Wagner, The relation between severe plastic deformation microstructure and corrosion behavior of AZ31 magnesium alloy, J. Alloys Compd. 468 (2009) 222–229, https://doi.org/10.1016/j.jallcom.2008.01.084.
[237] G.R.A. A, S.K.P. A, R.S.M.A. B, Effects of grain size on the corrosion resistance of wrought magnesium alloys containing neodymium, Corros. Sci. 58 (2012) 145–151, https://doi.org/10.1016/j.corsci.2012.01.021.
[238] R. Davis, A. Singh, K. Debnath, A.K. Keshri, P. Soares, L. Sopchenski, H.A. Terryn, V. Prakash, Surface modification of biodegradable Mg alloy by adapting EDM capabilities with cryogenically-treated tool electrodes, Int. J. Adv. Manuf. Tech. (2023), https://doi.org/10.1007/s00170-023-11395-0.
[239] L. Ling, S. Cai, Q. Li, J. Sun, X. Bao, G. Xu, Recent advances in hydrothermal modification of calcium phosphorus coating on magnesium alloy, J. Magnesium Alloys 10 (2022) 62–80, https://doi.org/10.1016/j.jma.2021.05.014.
[240] T. Bita, A. Antoniac, I. Ciuca, M. Miculescu, C.M. Cotrut, G. Paltanea, H. Dura, I. Corneschi, I. Antoniac, I.D. Carstoc, A.D. Bodog, Effect of fluoride coatings on the corrosion behavior of Mg-Zn-Ca-Mn alloys for medical application, Materials 16 (2023), https://doi.org/10.3390/ma16134508.
[241] I. Antoniac, V. Manescu, A. Antoniac, G. Paltanea, Magnesium-based alloys with adapted interfaces for bone implants and tissue engineering, Regen Biomater 10 (2023), https://doi.org/10.1093/rb/rbad095.
[242] C. Liu, M. Zhao, X. Song, D. Li, The comparative biological properties of $Mg^+$ or Ca+ implanted Cu-TiN nanocomposite coatings on titanium alloys, Vacuum 194 (2021), https://doi.org/10.1016/j.vacuum.2021.110618.
[243] F. Hussain, M.U. Manzoor, M. Kamran, M.T.Z. Butt, Surface modification of AZ31B magnesium alloy by anodization process, J. Pak. Int. Chem. Eng. 49 (2021) 11–20.
[244] M. Asaduzzaman Chowdhury, M.D. Helal Hossain, N. Hossain, Z. Hossen, M. Arefin Kowser, M. Masud Rana, Advances in coatings on Mg alloys and their anti-microbial activity for implant applications, A, J. Polym. Sci. 15 (2022), https://doi.org/10.1016/j.arabjc.2022.104214.
[245] W. Wang, K.W.K. Yeung, Bone grafts and biomaterials substitutes for bone defect repair: a review, Bioact. Mater. 2 (2017) 224–247, https://doi.org/10.1016/j.bioactmat.2017.05.007.
[246] G.S. Hikku, C. Arthi, R.B. Jeen Robert, K. Jeyasubramanian, R. Murugesan, Calcium phosphate conversion technique: a versatile route to develop corrosion resistant hydroxyapatite coating over Mg/Mg alloys based implants, J. Magnesium Alloys 10 (2022) 1821–1845, https://doi.org/10.1016/j.jma.2022.06.005.
[247] S. Huang, J. Li, K. Qin, Z. Wang, J. Yang, F. Cao, W. Li, Y. Liu, L. Liu, D. Zhao, Evaluation of the performance of Ca-deficient hydroxyapatite (CDHA)/$MgF_2$ bilayer coating on biodegradable high-purity magnesium in a femoral condyle defect model in rabbits, Regen Biomater 9 (2022), https://doi.org/10.1093/rb/rbac066.
[248] F. Peng, D. Wang, Y. Tian, H. Cao, Y. Qiao, X. Liu, Sealing the pores of PEO coating with Mg-Al layered double hydroxide: enhanced corrosion resistance, cytocompatibility and drug delivery ability, Sci. Rep. 7 (2017), https://doi.org/10.1038/s41598-017-08238-w.
[249] J. Wang, F. Peng, X. Wu, D. Wang, A. Zheng, L. Cao, C. Yu, X. Liu, X. Jiang, Biocompatibility and bone regeneration of PEO/Mg-Al LDH-coated pure Mg: an in vitro and in vivo study, Sci. China Mater. 64 (2020) 460–473, https://doi.org/10.1007/s40843-020-1392-5.
[250] B. Subramanian, P. Sasikumar, S.T. Rajan, K.G. Shankar, M. Veerapandian, Fabrication of Zr-Ti-Si glassy metallic overlay on 3D printed Ti-6Al4V implant prototypes for enhanced biocompatibility, J. Alloys Compd. 960 (2023), https://doi.org/10.1016/j.jallcom.2023.170933.
[251] A. Jabed, M.N. Bhuiyan, W. Haider, I. Shabib, Distinctive features and fabrication routes of metallic-glass systems designed for different engineering applications: a review, Coatings 13 (2023), https://doi.org/10.3390/coatings13101689.
[252] F.A. D'Yachenko, V.O. Semin, A.R. Shugurov, M.G. Ostapenko, L.L. Meisner, Nanobubbles and physical-mechanical properties of the Ti-Ni-Ta-Si-based metallic glass surface alloy fabricated on a TiNi SMA substrate by additive thin-film electron-beam method, Surf. Coat. Technol. 474 (2023), https://doi.org/10.1016/j.surfcoat.2023.130123.
[253] A.L. Greer, Y.H. Sun, Stored energy in metallic glasses due to strains within the elastic limit, Philos. Mag. A 96 (2016) 1–21, https://doi.org/10.1080/14786435.2016.1177231.

[254] H. Li, S. Pang, Y. Liu, L. Sun, P.K. Liaw, T. Zhang, Biodegradable Mg–Zn–Ca–Sr bulk metallic glasses with enhanced corrosion performance for biomedical applications, Mater. Des. 67 (2015) 9–19, https://doi.org/10.1016/j.matdes.2014.10.085.
[255] A. Jaafar, C. Hecker, P. Árki, Y. Joseph, Sol-gel derived hydroxyapatite coatings for titanium implants: a review, Bioengineering 7 (2020), https://doi.org/10.3390/bioengineering7040127.
[256] M. Rahman, Y. Li, C. Wen, HA coating on Mg alloys for biomedical applications: a review, J. Magnesium Alloys 8 (2020) 15, https://doi.org/10.1016/j.jma.2020.05.003.
[257] G.C. Gomes, F.F. Borghi, R.O. Ospina, E.O. López, A. Mello, Nd:YAG (532 nm) pulsed laser deposition produces crystalline hydroxyapatite thin coatings at room temperature, Surf. Coat. Technol. 329 (2017).